RESPONSE TO REVIEWER 1

The authors would like to thank Reviewer 1 for the comments and suggestions that have helped to improve the overall quality of the paper. In our answers, we have referred to the line numbers as in the marked-up manuscript version.

General comments:

One wonders why not other products have been consulted or why no attempt has been made to explore reasons for differences.

The NEMO-based Ocean Reanalyses (ORAs) used in this work, which are quite similar products among many different existing ORAs (as pointed by the reviewer), already show large differences in the South Atlantic meridional transports. Including more and different reanalyses would only add an extra factor – different models – to be accounted for in explaining differences. We also wanted to focus on a comparison between ORAs and Free-Running Models (FRMs) and to explore differences/similarities between them, so we use FRMs and ORAs with the same basic NEMO model. We think this dataset (totalling 6 products) allows to compare the ORAs and FRMs, as well as to explore the ORA transport differences in the South Atlantic.

We agree with the reviewer that more work is needed to properly investigate the reasons for the ORA differences, but we have considerably narrowed the problem to understand how to better constrain the western boundary transports. We have shown that the current ORAs do show good agreement in currents and transports in the interior which is a big step forward. We make clear in the conclusions that future work will address specifically this western boundary problem. We intend to use one specific ORA product and run sensitivity experiments changing the data assimilation configurations near the western boundary so that we have control over the product to better address the western boundary issue. Also because we do not have a good observational truth for these western boundary flows, in our opinion this needs a different approach, rather than intercomparison of current products, to continue the investigation. These next steps to fully pin down the reasons behind the inter-product spread represent a complete study in itself.

Details:

L72: How about the contribution from the eastern boundary and the interior circulation, wouldn't these be worth to be shown or at least be mentioned?

We agree with the reviewer about mentioning the interior and eastern boundary. Both are now mentioned in the sentence starting in L70, as below:

"Their result reveals the need for further assessment of the skills and uncertainties of the ORAs in the South Atlantic, such as comparing them with Free-Running Models (FRMs) and evaluating their SAMOC contributions across the eastern, interior, and western boundary regions shown in Fig. 1."

However, for Fig.1 we still focus on the western boundary circulation to set the scene, particularly for the analyses of Fig. 9, Fig. 10 and Fig. 11 in the section 3.3 showing the western boundary role in the large-scale transports.

L163: I am not clear which studies you refer to. There were already two named, and now two different follow. Maybe this be slightly rearranged that it reads smoother.

The sentence in L161 was rearranged as below:

"The large-scale transports are compared to the 34 high-density XBT-based estimates (XBT-AX18) in the Southern Atlantic from 2002 to 2013, with transport estimates at 35˚S and 30˚S given by Majumder et al. (2016). Recent observational studies are also used for comparison, which employ different methodologies to calculate the SAMOC and MHT between 35˚S and 20˚S, as follows: (i) an Argo climatology (Dong et al., 2014), (ii) altimetry synthetic profiles based on the correlation of the AVISO SLA and isotherm depths (Dong et al., 2015), and (iii) dynamic height fields from Argo and AVISO SSH (Majumder et al., 2016) are used together with wind fields to estimate the total transports."

Fig. 4g: Label g missing

Label g is now included in Fig. 4.

L258: Presumably these are the same areas that contribute most to the MHT. The trivial expectation is that the relative spread is similar, such that differences in areas that matter most for the mean MHT also matter most for their spread. Is this so? Could you check this, maybe show the ensemble mean p-OTT.

According to the plot below, areas of largest spread do correspond to areas with largest mean transports (i.e. along the western boundary).

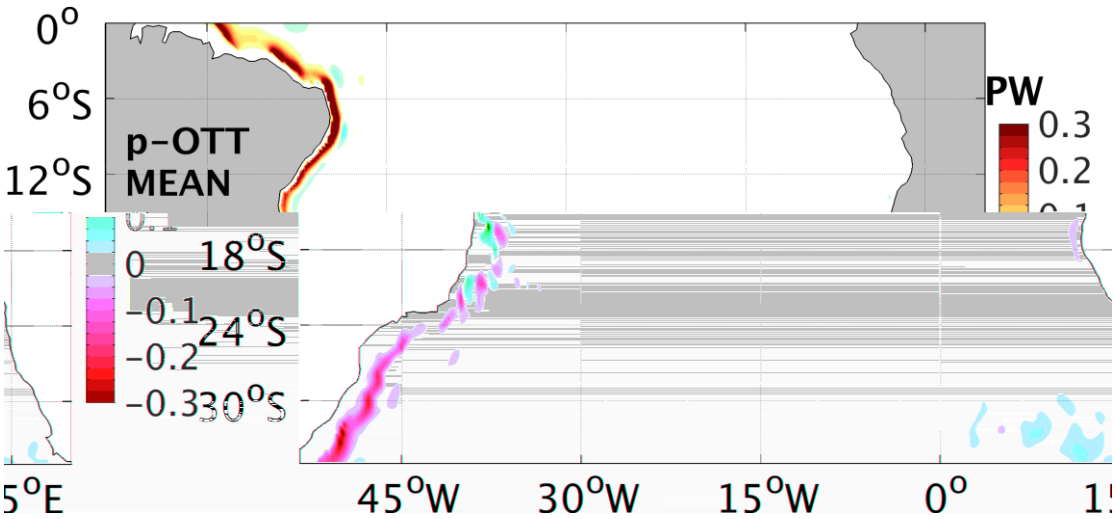

We now note it in the text, which has been changed in L257 as below:

"The $v\overline{T}$ component captures variations from ~0.2 PW to 1 PW (Fig. 7c), explaining ~83% of the total MHT spread which is mainly concentrated in the areas with largest mean transports, i.e. the narrow western boundary region (Fig. 7d)."

L274-278: Wouldn't you expect to see an impact of the second peak of southward transports in the ORAs that the FRMs should not show? Also, since Fig.4 shows the mean, I don't see how you can infer conclusions for the time variability from this. You could investigate the contributions to the heat transport variability in more detail instead of speculating.

The ORAs southward peak between 10˚S and 5˚S in the maps of Fig. 4 does actually increase their southward flow by ~4 Sv compared with the FRMs (see Fig. 4g). However their North Brazil Current (NBC) transports can increase from ~4 up to 9 Sv compared to the FRMs (see Fig. 5). So, the ORA second southward peak is more than balanced by the increase in the western boundary transports, and this is why there are no clear sings of it in Fig. 2a or in Fig. 3c.

Answering the second part of the reviewer's question, the interior southward flow increases towards the equator for all products, reaching similar magnitudes to the overturning component, and with both having similar ΔTs. So it is natural to expect that variations in the southward flow will also contribute to the MHT variability in this region. This is all that was intended. Further investigation of this time variability would be possible but is not the main focus of this paper. The sentence is now modified in L276 as below:

"Therefore it is likely that these large upper level tropical circulations explain why ψ_{max} does not dominate the MHT variability close to the equator, as also noted by Valdivieso et al. (2014). "

L293-294: I think showing the ensemble mean p-OTT would also serve here to make this point. Fig. 1 shows the volume transport but the depth integrated heat transport could be different.

We have added this figure in answer to L258 above but we do not see how it is relevant to this point? The main point of Fig. 9 is to show the continuous band of positive MHT regression coefficients against the western boundary which means that ORAs with the largest MHTs must show less southward transport along the Brazil Current (BC) and higher northward transport along the NBC, compared to the FRMs. This pattern is further confirmed by Fig. 10 for both BC and NBC.

L299-300: It would be nice to add information on these limits to the figure caption or state them somewhere else.

We agree with the reviewer. The water masses limits are now stated in the captions of Fig. 10:

"The TW, SACW and AAIW limits are defined in kg m^{-3} with $\sigma < 25.5$, $25.5 \leq \sigma < 27.1$, and $27.1 \leq \sigma < 27.3$, respectively."

L315-317: Isn't this basically what we already know from Figure 2?

In Fig. 2 we show the AMOC strength across the basin which is a zonally integrated quantity. In the lines here we discuss the 4-box model of the transports (Fig. 11), i.e. the transports are broken down into western boundary versus interior, and into upper versus deep circulations. We agree that main difference between the products is shown in Fig. 2 but it cannot be really understood. Fig. 11 shows where the inter-product compensations occur and how the 4-box transports are balanced within products. We therefore say that GLORYS2V4 and UR025.4 are ~10 Sv and 8.5 Sv larger than ORCA025 in the upper western boundary, and these inter-product differences are mostly compensated by the deep western boundary transports. In Fig. 11, we can also see the contributions and their much better agreement from the interior boxes.

L334-335: Can this variability be considered realistic? Are the associated features similar to the high resolution model simulation? For instance, the ORAs, except ORAP5, have substantially more variability in the interior than the eddy resolving model.

Masina et al. (2015) also found that these NEMO reanalyses show an increased Eddy Kinetic Energy (EKE) and that they are in much better agreement with the OSCAR estimates when compared to no-assimilation runs. GLORYS, CGLORS and UR025-4, which have the largest transport variability here, also show the best level of agreement with OSCAR. This is an indication that the higher ORA variability caused by DA in the velocity fields is consistent with information inferred from observations. We have tried to be more specific changing the text in L334 as below:

"Figures 12a-f show that the interannual variability in p-OTTs is larger in the ORAs and in the high resolution ORCA0083 than in ORCA025. The assimilation of observations in eddy-permitting models introduces variability that would otherwise only appear with higher resolution, as in ORCA0083. According to Masina et al. (2015), this higher variability in the ORAs is in better agreement with the Eddy Kinetic Energy estimates from the ocean surface current velocities (OSCAR) product than that of the FRMs."

L353-355: It does not become clear why these two time series are shown together. What is their relation or the intention here?

The intention is to verify how these two components of the circulation behave over time in the tropical South Atlantic. For example, how are these transports in the ORAs impacted by the introduction of Argo? From Fig. 13 the southward interior flow is better constrained by the ORAs in the later years, related with the assimilation of a larger number of (Argo) hydrographic observations (including salinity observations) across the basin. However, the overturning component is dominated by the narrow western boundary and the lack of observations in these narrow areas means the overturning is not better constrained, and so the ENS-ORA spread of the overturning component remains nearly steady over time.

RESPONSE TO REVIEWER 2

The authors would like to thank Reviewer 2 for the comments and suggestions that have helped to improve the overall quality of the paper. In our answers, we have referred to the line numbers as in the marked-up manuscript version.

General comments:

Much of it is either unsurprising (ORAs are closer to observations than FRMs) or under-explored (what needs to be done in the ORAs to better represent the boundary currents).

We provide a comprehensive analysis showing where the differences between these products come from (i.e. the western boundary currents). The results make sense in relation to the data that have been assimilated. Although the results are perhaps not surprising, they had not be shown with this level of clarity in previous studies. In addition, the consistent impact of assimilation on the interior circulations in multiple products has not been previously shown. The comparison with the FRMs clearly shows that ORAs have additional circulation differences relative to the FRMs in the basin interior.

We agree with the reviewer that there is more work to be done in order to fully understand the reasons for the ORA differences at the western boundary. However, this requires a full study in itself. A different approach making sensitivity experiments in the South Atlantic with a single ORA, changing for example data assimilation configurations and assimilated observations near the western boundary, is needed to make further progress. This is currently being done and will hopefully come out as the future paper.

Just from reading the manuscript, it is not clear how this study is different from the Majumder et al. (2016) paper. This needs to be better highlighted in the introduction section.

Majumder et al. (2016) have used ORAs and observational estimates to study the meridional transports in the Southern Atlantic. However, their study does not go further than showing that the transport magnitudes between ORAs as well as between ORAs and observations show large discrepancies. Motivated by Majudmer et al. (2016), we show here more details of the ORA transport differences and interpret the impact and limitations of the DA schemes in improving the South Atlantic circulation, also through the inclusion of FRMs with distinct spatial resolutions. For example, we clearly demonstrate the dominant role of inter-product spread in velocity, and the limited contribution of inter-model spread in temperature. This is now better highlighted in the text - L71 and L83 - as below:

L70: “Their result reveals the need for further assessment of the skills and uncertainties of the ORAs in the South Atlantic, such as comparing them with Free-Running Models (FRMs) and evaluating their SAMOC contributions across the eastern, interior, and western boundary regions shown in Fig. 1.”

L82: “Going further than Majumder et al. (2016), we also narrow down these transport differences in an attempt to understand the potential impact (and limitations) of the DA schemes in improving the ORA states in the South Atlantic.”

It would be good to discuss the findings, especially that the models so poorly represent the boundary currents, in relation to OSSEs; i.e. which measurements are needed (and where are they needed) to improve the ORAs?

We have now included more discussion about model sensitivity studies and possible OSSEs. The text has been changed in L400 as below:

“Observation system simulation experiments (OSSEs) with AMOC trans-basin arrays have shown that the meridional flow strength can be sensitive to the number of hydrographic profiles near the boundaries in both North (e.g. Hirschi et al., 2003; Baehr et al., 2004) and South Atlantic (e.g. Perez et al., 2011). The combined assimilation of open ocean hydrographic observations and the continuous RAPID array western boundary measurements have also been shown to locally improve the AMOC strength at 26.5˚N (Stepanov et al., 2012). This emphasises the role that more systematic observations located at the eastern and western boundaries at several latitudes may play in monitoring the AMOC (Marotzke et al., 1999). In the future, the SAMOC observing system (Ansorge et al., 2014; Hummels et al., 2015), which will provide time series of NBC measurements at the western boundary at 11˚S, could be assimilated into the ORAs to constrain the regions of largest spread in the tropical South Atlantic.”

I was surprised to read that the ORAs are much less constrained before the 2000s, yet the authors chose to use the 1997-2010 period for their analysis. Why not start after the Argo era begins then? And why not include later years; 2010 is seven years ago! That would make much more sense to me.

The UR025.4 reanalysis ends in 2010, so we took 2010 as the final year of the chosen period. In addition, the plot below show that meridional transport differences for the periods 1997-2010 (solid lines) and 2000-2010 (dashed lines) are quite small.

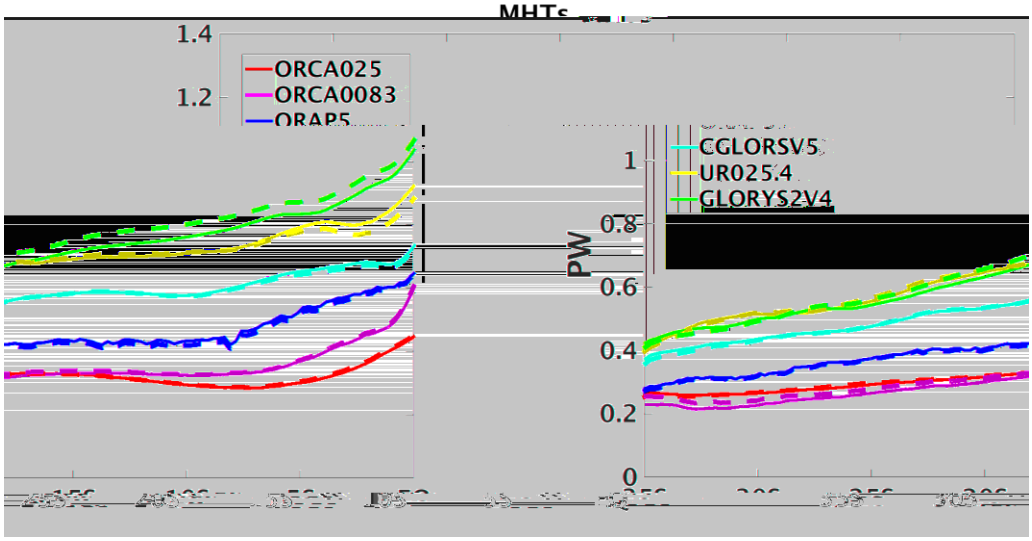

Including some years before the Argo period also allows us to show that the ORA interior circulation is better constrained after the Argo begins (see Fig. 13), whereas the overturning spread between them remains steady over time. If we had only used Argo period results we would have had few averaging years. We have modified the paragraph in L153 as below:

"In order to avoid any dynamical spin-up in the early years of the simulation for products starting in the late eighties or early nineties (e.g. UR025.4 and GLORYS2V4), and because UR025.4 ends in 2010, a common time period from 1997 to 2010 is chosen. Despite the fact that subsurface ocean observations are scarcer before the 2000s (i.e. prior to the full deployment of Argo floats), the total meridional transports for the periods 1997-2010 and 2000-2010 do not differ significantly. "

The authors need to state much more clearly which of the observational data they use to assess the skill of the models have gone into the ORAs themselves, i.e. is the XBT-AX18 line, or WOA13, used in the data assimilation process of the ORAs? In other words, are these independent validations?

We agree with the reviewer about this comment and this is now clearly mentioned in a new paragraph starting in L174:

"Of the observational estimates above, the XBT-AX18 line is not independent as it is included in the EN3 and EN4 datasets which are assimilated by the ORAs (see Tab.1). Although WOA13 is not directly assimilated by the ORAs, it uses the same observational information as EN3 and EN4, and so it also cannot be treated as completely independent."

There could be more discussion of the features seen in the Cape Basin. Where do these come from? How are they related to MOC and the Brazil Current? Are they noise or signal?

From checking spatial animations of SLA in the Cape basin as well as maps of Eddy Kinetic Energy for the products, it is clear that there are differences in reproducing the Agulhas rings between the FRMs and ORAs, as well as between the ORAs. This implies that the Cape basin variability impacts the ENS-ORA and ENS-ALL transport spreads (Fig. 9). This may be related to the way SLA is assimilated into the ORAs, see added discussion:

L288: "South of 25˚S the p-OTT contributions to the total MHT are more distributed, with a noticeable contribution from the Agulhas leakage caused by the different intensity and positioning of the Agulhas rings between the products as they travel westward across the Cape basin."

L346: "The different levels of variability in the Agulhas leakage between ORCA025 and ORAs may be attributed to the impacts of the SLA assimilation (Backeberg et al., 2014). However, even between ORAs these Agulhas patterns differ, e.g. the weaker contributions in ORAP5 may be due to smoothing from the super-observation method applied to the altimeter data (Mogensen et al., 2012), as also noted by Masina et al. (2015)."

For a study that focusses so much on boundary currents, it is surprising that there is no mention of how the boundary conditions have been implemented in the models? Are these all the same? Partial slip? What parameters have been used? Is there any relation between the way the boundary conditions are implemented and the skill of the ORAs/FRMs?

We agree with this comment and information about the lateral boundary conditions for all the products are now given in the text:

L121: "Both ORCA0083 and ORCA025 employ a free-slip (no-stress) configuration for the lateral momentum boundary conditions."

L148: "On lateral boundaries, UR025.4 and ORAP5 adopt a free-slip configuration whereas CGLORSV5 and GLORYS2V4 employ a partial-slip condition. In the latter, the constant of proportionality (α) between the tangential stress and the tangential velocity is defined as 0.5 for both products."

Some further discussion has been added in L394 with respect to the lateral boundary conditions:

"It is noteworthy that the lateral boundary conditions in the ORAs and FRMs vary between free-slip (α=0) and partial-slip (α=0.5). However, there is no clear correspondence between the choice of lateral boundary conditions and the strength of the western boundary transports, with free-slip products (e.g. UR025.4) having similar transports to partial-slip products (e.g. GLORYS2V4)."

Minor issues:

- line 14: Start the abstract with a sentence about why the South Atlantic is relevant? The introduction section starts with a few good paragraphs, and these might be summarised at the beginning of the abstract?

The abstract now starts with the following sentence:

"The Meridional Heat Transport (MHT) of the South Atlantic plays a key role in the global heat budget: it is the only equatorward basin-scale ocean heat transport and it sets the northward direction of the global cross-equatorial transport."

We also thought we could better improve the abstract as a whole, making it easier to understand for a broader number of readers. So you will find a few changes and text rearrangements there.

- line 49: Add 'possibly' before 'leading' ?

Done.

- line 65: Explicitly state that most ORAs lack dynamical consistency?

We have removed the word "dynamically" from the ORA definition in L64. We think this is enough to meet the reviewer's requirement.

- line 113: I thought most NEMO models were z*?

For all the NEMO-based products used here, the code versions with fixed z-levels and partial cell topography are used. There are additional challenges in implementing DA (especially altimetry) with z*.

- line 119: What do 'W', 'SAT' and 'SAH' stand for?

These acronyms are defined in L106 and L107:

"The ERA-Interim reanalysis provides Winds (W) at 10 m, Surface Air Temperature (SAT) and Surface Air Humidity (SAH) at 2 m, daily Radiative Fluxes (RF) and Precipitation (P) fields…"

- line 263: Why is this interpretation made? What is the motivation for this?

There is a clear line of spread in the p-$\bar{v}T$ right against the western boundary (Fig. 7f). This might indicate that local response to small temperature changes on the western boundary slope may largely determine the meridional transport variability in ocean models through changes in the western boundary current velocities (p-$v\bar{T}$; Fig. 7d), as already stated by Bingham and Hughes (2009) for the North Atlantic (as discussed in the paper in L390).

- Figure 2: How is 'spread' defined here? Highest-lowest? Standard deviation?

The spread is defined as the standard deviation between the products. To make this point clear, we have added this information to the caption of Fig. 2:

"(a) The AMOC strength ψ_{max} (Sv) averaged over 1997-2010 as a function of latitude, and (b) its spread (Sv) defined as the standard deviation of the ENS-ALL and ENS-ORA."

- Figure 3: Why does the size of the horizontal lines on the whiskers vary? What does this mean?

The horizontal lines on the whiskers do not mean anything relevant. However, the size of these horizontal lines in Fig. 3c were adjusted to be the same size.

- Figure 5: How is the standard error defined here?

It is defined as the standard deviation divided by the square root of the length of the monthly time series. The caption of Fig. 5 is now changed to include the following information:

“The black bars represent the standard errors where the size of the sample is defined as the length of the monthly time series.”

- Figure 8: What is the relevance at this line of 0.7 correlation? Is this significance level? How calculated?

We have removed the 0.7 line from the figure to avoid any kind of misunderstanding. In Fig. 8, we compute Pearson correlations calculated with 95% significance level on a monthly time scale. This information is now added to the caption of Fig. 8:

“The monthly Pearson correlation between the SAMOC strength and the MHT as a function of latitude for 1997-2010, calculated with significance level of 95%. “

- Figure 11: What do the dashed circles represent above the top two bar charts?

It was an attempt to say that in the tropical South Atlantic the northward upper western boundary has part of its transports to compensate for the southward deep western boundary flow (solid circles), and other part to compensate for the southward upper interior flow (dashed circles). However, we have removed the dashed circles in order to avoid any kind of misunderstanding.

- line 29: The word ‘right’ is confusing here, as it might also be interpreted as the right (as opposed to left) side of the plots?

We have removed the entire sentence of L26 since we have changed the abstract as a whole.

- line 81: ‘Focusing on’ and line 412: ‘near the boundaries’

Done.

- line 267: Is this correlation R or R^2?

R.

South Atlantic meridional transports from NEMO-based simulations and reanalyses

Davi Mignac[1,2], David Ferreira[2], and Keith Haines[2]

[1]*Postgraduate Program in Atmosphere, Oceans and Climate, University of Reading, Reading, UK*
[2]*Department of Meteorology, University of Reading, Reading, UK*

Correspondence to: Davi Mignac (d.mignaccarneiro@pgr.reading.ac.uk)

Abstract

The Meridional Heat Transport (MHT) of the South Atlantic plays a key role in the global heat budget: it is the only equatorward basin-scale ocean heat transport and it sets the northward direction of the global cross-equatorial transport. Its strength and variability however are not well known. The South Atlantic ~~meridional~~ transports are evaluated for four state-of-the-art global Ocean Reanalyses (ORAs) and two Free-Running Models (FRMs) in the period 1997-2010. All products employ the Nucleus for European Modelling of the Oceans model, and the ORAs share very similar configurations. Very few previous works have looked at ocean circulation patterns in reanalysis products, but here we show that t~~T~~he ORA basin interior transports are consistently ~~modified~~ improved by the assimilated in situ and satellite observations, relative to the FRMs, especially in the Argo period~~, with an improved representation of the south equatorial currents~~. The ORAs also exhibit systematically higher meridional transports than the FRMs, in closer agreement with ~~large scale~~ observational estimates at 35˚S and ~~western boundary measurements at~~ 11˚S. However, the ~~transport~~data assimilation impact~~s by data assimilation~~ on the meridional transports still greatly varies~~y~~ between the ORAs, leading to differences up to ~8 Sv and 0.4 PW in the South Atlantic Meridional Overturning Circulation and the ~~Meridional Heat Transports (~~ MHTs~~)~~, respectively. We narrow this down to l~~L~~arge inter-product discrepancies ~~arise~~ in the ~~ORA~~ W~~w~~estern B~~b~~oundary C~~c~~urrents (WBCs) at both upper and deep levels explaining up to ~85% of the inter-product differences in ~~their total~~ MHT~~s.,~~ We show that ~~and~~ meridional velocity differences, rather than temperatures differences, in the WBCs drive ~83% of this MHT spread. ~~Further analysis shows that only very confined temperature differences right against the western boundary geostrophically explain the large boundary current velocity differences.~~ These findings ~~suggest~~ show that the ~~current~~ present ocean observation network and data assimilation schemes~~, even with Argo data,~~ can be used to consistently constrain the South Atlantic ~~basin~~ interior circulation ~~in the ORAs~~,

but not the overturning ~~transport~~ component which is dominated by the narrow western boundary currents. ~~as in the South Atlantic.~~ This will likely limit the effectiveness of ORA products for climate or decadal prediction studies.

1. Introduction

An important feature of present-day climate is that the heat transport in the Atlantic Ocean is northward in both hemispheres, rather than poleward as in the Indo-Pacific Ocean (Ganachaud and Wunsch, 2003) and in the atmosphere (Trenberth and Caron, 2001). The South Atlantic acts as a communicator between the southern and northern oceans (Garzoli and Matano, 2011), through the Meridional Overturning Circulation (MOC) transporting warm water northward across the equator to compensate for the southward export of colder North Atlantic Deep Water (NADW).

The northward upper limb of the South Atlantic MOC (hereafter SAMOC) is a complex mixture of water masses originating from the Indian, Pacific and Southern oceans, which are blended together in the South Atlantic gyre circulations. The water mass redistribution in the South Atlantic and the interocean exchanges can significantly influence the long-term Atlantic MOC (hereafter AMOC) variability (Garzoli and Matano, 2011), particularly on decadal time scales through the heat and salt export by the Agulhas leakage (Weijer et al., 2002; Sebille et al., 2011). The SAMOC salt fluxes at 35˚S have also been suggested to reflect the MOC stability in climate models (Drijfhout et al., 2011; Hawkins et al., 2011). In the case where the SAMOC imports salt into the Atlantic basin, a weakening of the AMOC would be followed by a further freshening of the basin, a positive feedback possibly leading to the collapse of the AMOC.

Marshall et al. (2013) argue that the northward ocean heat transport across the equator sets the mean position of the Inter-tropical Convergence Zone in the northern hemisphere. Since the South Atlantic is the only major ocean basin that transports heat equatorward, quantifying and understanding the SAMOC should help to explain the inter-hemispheric heat exchanges and improve interannual-to-decadal climate simulations, as also recently reinforced by Lopez et al. (2016). For this reason, a SAMOC observing system has already been initiated in 2002 with quarterly high-density eXpendable BathyTermograph (XBT) lines at 35˚S (Garzoli and Baringer, 2007), and recently with the development of the South Atlantic MOC Basin-wide Array (SAMBA; Ansorge et al., 2014), analogous to the RAPID array in the North Atlantic (Cunningham et al., 2007).

However, the lack of long term measurements in the area still limits our understanding of the South Atlantic state and its variability, reflecting the large disagreement between ~~both~~ observational and model studies (Garzoli et al., 2013; Dong et al., 2014; Dong et al., 2015; Majumder et al., 2016; Stepanov et al., 2016).

In this context, Ocean Reanalyses (ORAs; Balmaseda et al., 2015) could be useful tools to monitor the ocean circulation and change indicators (Masina et al., 2015; Palmer et al., 2015). The ORAs employ Ocean General Circulation Models (OGCM) and Data Assimilation (DA) schemes to synthetize a diverse network of available ocean observations in order to arrive at a ~~dynamically~~ consistent estimate of the historical ocean state. In such products, atmospheric forcing combined with DA are used to dynamically extrapolate the observational information to regions without observations, which gives the ORAs the potential to provide complete, time-evolving descriptions of the ocean state and its circulation.

In the South Atlantic, ORA diagnostics have been put together with three-dimensional velocity fields constructed from Argo and Sea Surface Height (SSH) observations to study the SAMOC variability and its relation with the Meridional Heat Transports (MHT) between 35˚S and 20˚S (Majumder et al., 2016). Although both observations and ORAs show strong correlations between the SAMOC and MHT, Majumder et al. (2016) also found significant discrepancies in the transport magnitudes between the ORAs as well as between the ORAs and the observations. ~~T~~heir~~is~~ result reveals the need for further ~~more comprehensive studies to~~ assessment of the skills and uncertainties of the ORAs in the South Atlantic, such as comparing them with Free-Running Models (FRMs) and evaluating their SAMOC contributions across the eastern, interior, and western boundary regions shown in Fig. 1.~~, considering the complex western boundary dynamics and their contribution to the SAMOC transports (Fig. 1).~~

The next generation of operational climate prediction systems will implement eddy-permitting ocean models, and it is expected that ORAs will provide improved initial conditions for such climate prediction models. The comparison between ORAs and ~~Free-Running Models (~~FRMs~~)~~ is a critical step in assessing the feasibility of initialising the ocean transports which are not directly observed. Such intercomparisons therefore can give valuable insights about how the transports are affected by DA (e.g. Zuo et al., 2011; Karspeck et al., 2015). To address these issues, we use ~~here~~ state-of-the-art ORAs at eddy-permitting resolution with two FRMs at eddy-permitting and eddy-resolving resolutions to study the meridional transports in the South Atlantic between 35˚S and the equator ~~(Fig. 1)~~. Focusing on the meridional volume and heat transports, we first identify

similarities and differences between products. ~~In a second step~~Going further than Majumder et al. (2016), we also ~~analyse~~ narrow down ~~the underlying causes of~~ these transport differences in an attempt to understand the potential impact (and limitations) of the DA schemes in improving the ~~simulated~~ ORA states in the South Atlantic.

The paper is organised as follows. In Section 2 a brief overview of the dataset configurations is presented. Sections 3.1 and 3.2 show the results of the time mean transports and the contributions of the temperature (T) and meridional velocities (v) to the spread in the heat transports, respectively. Section 3.3 evaluates the western boundary role in the South Atlantic large-scale transport discrepancies between the products. Section 3.4 ends the results section with the time variability of the transports. Section 4 contains the discussion and conclusions.

2. The dataset

In this study, we use outputs from two FRMs and four ORAs, each with a global domain. All the products are configured with the Nucleus for European Modelling of the Oceans (NEMO; Madec, 2008) model, coupled to the Louvain la Neuve sea-ice model version 2 (LIM2; Timmermann et al., 2005). The former is a state-of-the-art primitive equation z-level model employing both hydrostatic and Boussinesq approximations, whereas the latter is a dynamic-thermodynamic sea-ice model specifically designed for climate studies. For this dataset, NEMO is configured with a partial cell topography (Adcroft et al., 1997), and a quasi-isotropic tripolar ORCA grid (Madec and Imbard, 1996). Sub-sections listing the main characteristics of the FRMs and ORAs are presented below. Tab.1 compares the main configurations of each product.

2.1 Free-running models

The standard configurations of the FRMs at 1/4˚ and 1/12˚ horizontal resolution used in this study have been setup within the DRAKKAR consortium (e.g. Barnier et al., 2006; Penduff et al., 2007, 2010; Treguier et al., 2014; Marzocchi et al., 2015). The FRM at 1/4˚ horizontal resolution is referred to here as ORCA025 and has 46 z-levels, with thickness ranging from 6 m at the surface to 250 m at the ocean bottom. ORCA025 is forced by the ERA-Interim atmospheric reanalysis product (Simmons et al., 2007) from the European Centre for Medium-Range Weather Forecasts (ECMWF). The ERA-Interim reanalysis provides Winds (W) at 10 m, Surface Air Temperature (SAT) and Surface Air Humidity (SAH) at 2 m, daily Radiative Fluxes

(RF) and Precipitation (P) fields, which are used to compute 6-hourly turbulent air/sea fluxes using the Large and Yeager (2004, 2009) bulk formulae. The integration of this ORCA025 setup was conducted at the University of Reading and is described in Haines et al. (2012) and Stepanov and Haines (2014) as the free control run associated with reanalysis UR025.3, and its initial condition is derived from a previous 1/4˚ run with hydrographic data assimilation (Smith and Haines, 2009). A moderate relaxation of Sea Surface Salinity (SSS) is applied towards Levitus (1998) with a time scale of approximately 180 days.

The FRM at 1/12˚ horizontal resolution (ORCA0083) has 75 z-levels. Its vertical grid is refined at the surface (1 m for the first level), smoothly increasing to a maximum thickness of 200 m at the bottom. The integration of ORCA0083 was performed by the Marine Systems Modelling group at the National Oceanography Centre, Southampton ~~(NOCS)~~, and is described in Marzocchi et al. (2015). The DRAKKAR Surface Forcing Set 4.1 (DFS4.1) or Set 5.1 (DFS5.1) is employed depending on the time period as shown by Tab.1. As detailed in Brodeau et al. (2010), DFS combines elements from two sources: (i) the Coordinated Ocean Research Experiments (CORE) forcing dataset, from which daily RF and monthly P are extracted; and (ii) ECMWF products from which W, SAT and SAH fields are taken. As in ORCA025, 6-hourly momentum and heat turbulent fluxes are computed in ORCA0083 following Large and Yeager (2004, 2009). ORCA0083 is initialised from Levitus (1998) climatology and applies the same SSS restoring term as in ORCA025. Both ORCA0083 and ORCA025 employ a free-slip (no-stress) configuration for the lateral momentum boundary conditions.

2.2 Ocean Reanalyses

The MyOcean global ocean reanalysis activity provided a series of global ORAs at eddy-permitting resolution (1/4˚) constrained by assimilation of observations and covering the "altimetric era" (i.e. period starting with the launch of TOPEX POSEIDON and ERS-1 satellites at the end of 1992). Four of these ORAs are considered in this work, namely: (i) The Ocean Reanalysis Pilot 5 (ORAP5; Zuo et al., 2015) from ECMWF; (ii) The Global Ocean Reanalysis System version 5 (CGLORSV5; Storto and Masina, 2016) from the Centro Euro-Mediterraneo sui Cambiamenti Climatici (CMCC); (iii) The University of Reading Reanalysis Version 4 (UR025.4, Valdivieso et al., 2014); and (iv) The Global Ocean Reanalysis and Simulation Version 4 (GLORYS2V4; CMEMS, 2017) from Mercator Ocean. These ORAs employ different state-of-the-art

ocean DA systems, which assimilate, in distinct ways, reprocessed observations of Sea Level Anomaly (SLA), Sea Surface Temperature (SST), in situ T and Salinity (S) profiles, and Sea Ice Concentration (SIC). The main references of the ORA DA schemes and their assimilated observations can be found in Tab.1 The vertical discretisation of GLORYS2V4, ORAP5 and UR025.4 follows exactly the same configuration as in ORCA0083 with 75 z-levels. CGLORSV5 has 50 z-levels in a similar configuration to ORCA025.

All the ORAs are forced with the ERA-Interim atmospheric reanalysis product from ECMWF. The turbulent air-~~/~~sea fluxes were calculated using the same methodology as in the FRMs, but their input into NEMO varies between 3 and 6-hour sampling depending on the product (see Tab. 1). In GLORYS2V4, large-scale corrections of the atmospheric forcings are also applied (Garric and Verbprugge, 2010), whereas in ORAP5 the impact of surface wave forcing on the ocean mixing and circulation is included (Janssen et al., 2013).

The relaxation strategies differ between the ORAs. In ORAP5 and CGLORSV5, the SST data in Tab. 1 are used to correct the turbulent heat fluxes, with a restoring term of -200 W m^{-2} K^{-1}. Their SSSs are also relaxed towards the World Ocean Atlas 2009 (WOA09; Locarnini et al., 2010) for ORAP5, and towards the UK Met Office ENhAnced ocean data assimilation and ClimaTe prediction (ENACT/ENSEMBLES) EN4 dataset (Good et al., 2013) for CGLORSV5, with time scales of approximately 300 days. No global SST and SSS restoring strategies have been implemented in UR025.4 and GLORYS2V4, and the only surface restoring mechanism is through the increments introduced by data assimilation itself. As also seen in Tab.1, the initialisation and spin-up differ between the ORAs. On lateral boundaries, UR025.4 and ORAP5 adopt a free-slip configuration whereas CGLORSV5 and GLORYS2V4 employ a partial-slip condition. In the latter, the constant of proportionality (α) between the tangential stress and the tangential velocity is defined as 0.5 for both products. More specific details comparing these NEMO-based ORAs can be found in Masina et al. (2015).

In this work, monthly averages of each product are used. The use of monthly means mitigates possible jumps introduced by incremental assimilation over a time window of several days. ~~A common time period from 1997 to 2010 is chosen~~ In order to avoid any dynamical spin-up in the early years of the simulation ~~from some~~for products starting in the late eighties or early nineties (e.g. UR025.4 and GLORYS2V4), and because UR025.4 ends in 2010, a common time period from 1997 to 2010 is chosen. Despite the fact that ~~Additionally,~~ subsurface ocean observations are scarcer before the 2000s (i.e. prior to the full

deployment of Argo floats), ~~and a more recent period is selected to consistently assess the product uncertainties and their variability.~~ the total meridional transports for the periods 1997-2010 and 2000-2010 do not differ significantly.

2.3 Observational estimates and surface heat flux products

The large-scale transports are compared to the 34 high-density XBT-based estimates (XBT-AX18~~; Garzoli and Baringer, 2007~~) ~~and recent observational studies~~ in the Southern Atlantic~~. The 34 repeat XBT cruises~~ from 2002 to 2013, with ~~have~~ transport estimates at 35˚S and 30˚S given ~~from~~ by Majumder et al. (2016). ~~The~~ Recent observational studies are also used for comparison, which employ different methodologies to calculate the SAMOC and MHT between 35˚S and 20˚S, as follows: (i) an Argo climatology (Dong et al., 2014), (ii) altimetry synthetic profiles based on the correlation of the AVISO SLA and isotherm depths (Dong et al., 2015), and (iii) dynamic height fields from Argo and AVISO SSH (Majumder et al., 2016) are used together with wind fields to estimate the total transports. The MHT based on integrating the Liu et al. (2015) surface heat flux product southward of 80˚N is also computed for the 1997-2010 period. This product uses top of atmosphere net radiation flux from CERES modified by the ERA-Interim atmospheric transports. ~~Finally, T~~the North Brazil Current (NBC) transports from 2000 to 2004 (Schott et al., 2005) and from 2013 to 2014 (Hummels et al., 2015) are also included for comparison. These NBC estimates are based on high-frequency velocity measurements from a moored western boundary array section located at 11˚S. Finally, WOA13 temperatures (Locarnini et al., 2013) from 1995 to 2012 are also compared with the temperatures from the ORAs and FRMs.

Of the observational estimates above, the XBT-AX18 line is not independent as it is included in the EN3 and EN4 datasets which are assimilated by the ORAs (see Tab.1). Although WOA13 is not directly assimilated by the ORAs, it uses the same observational information as EN3 and EN4, and so it also cannot be treated as completely independent.

3. Results

3.1 Time-mean transports

Figure 2a shows the time mean AMOC strength for each product, defined as the maximum (ψ_{max}) of the AMOC stream function at each latitude in the Atlantic basin. The ensemble spreads of ψ_{max} for all products (ENS-ALL hereafter) and for

only the ORAs (ENS-ORA hereafter) are shown in Fig. 2b. The discrepancies in AMOC strength between the ORAs are largest in the South Atlantic, reaching the maximum spread of 3.5 Sv (ENS-ALL) and 3 Sv (ENS-ORA) in the area between 20˚S and the equator. The two FRMs are similar to each other, both with relatively low AMOC across the basin. The assimilation of observations in the reanalyses appears to increase the AMOC strength at all latitudes. In the North Atlantic, especially in the subpolar gyre north of ~35˚N, the ORA AMOCs are consistently 3-4 Sv higher than in the FRMs. However, the increase of the ORA AMOCs is less consistent south of 35˚N, especially in the South Atlantic where the differences in the SAMOC transports can reach up to ~8 Sv between GLORYS2V4 and ORAP5. The latter is the ORA that has the lowest transports in the South Atlantic, closest to the FRMs.

Comparison with observational estimates at 35˚S (Figs. 3a-b) suggests that both the SAMOC strength and MHT of the ORAs are more realistic than those of the FRMs. However, even the highest MHTs of UR025.4 and GLORYS2V4 are almost 0.1 PW lower than the lowest observational estimate from Dong et al. (2015). The MHT underestimation of the FRMs and ORAs relative to the observations at 35˚S has already been reported by several authors (e.g. Dong et al., 2011a; Dong et al., 2011b; Perez et al., 2011; Sitz et al., 2015; Majumder et al., 2016; Stepanov et al., 2016). The black bars in Figs. 3a-b show monthly variability in the ORAs, but quarterly (XBT-AX18), monthly (Dong et al., 2014), weekly (Dong et al., 2015) or daily (Majumder et al., 2016) time scale variability in the observations. These clearly overlap each other although they cannot be regarded as uncertainties in the means. Despite their lower mean transports, the temporal variability of the FRMs is similar to that of the ORAs at 35˚S, around ± 0.3 PW and 3.0 Sv.

As in the SAMOC strength (Fig. 2), the inter-product spread in MHT gets larger towards the equator, with differences up to 0.4 PW between GLORYS2V4 and ORAP5 (Fig. 3c). The Liu et al. (2015) surface flux based product suggests higher heat transports in good agreement with UR025.4 and GLORYS2V4 across the South Atlantic basin, although the surface integration method accumulates errors from all higher latitudes. Liu et al. (2015) estimates also reasonably agree with the XBT-AX18 and other South Atlantic observational studies at 35˚S and 30˚S. However, the observational estimates diverge north of 30˚S, with the transports from Dong et al. (2015) and Majumder et al. (2016) differing by ~0.7 PW at 20˚S. These discrepancies underscore the uncertainties in observed transports through the South Atlantic.

Figures 4a-f show maps of the east-west accumulated volume transports from the surface down to the depth of ψ_{max} (typically ~1000 m) for each latitude, defined hereafter as z_{max}. These contours can be regarded as streamlines of the upper ocean gyre circulations. The northern boundary of the subtropical gyre (dashed contour of zero transport), near 20˚S and 15˚S, agrees well between products, with only GLORYS2V4 extending slightly further north. The subtropical gyre to the south is only partially shown but the strength of this gyre is quite consistent between the ORAs and ORCA0083, and significantly stronger than in ORCA025. The large-scale circulation equatorward of 15˚S is dominated by a southward flow increasing westwards until the strong northward NBC flow is reached in a very narrow western boundary area. The ORA southward flow in the basin interior ranges between -14 and -18 Sv. For consistency with the overturning strength ψ_{max} (represented in Figs. 4a-f by the westernmost accumulated transports), the NBC region typically reaches ~36 Sv of northward flow. This agrees with other studies of the role of the NBC in the AMOC upper branch crossing the equatorial Atlantic (e.g. Rabe et al., 2008; Sebille et al., 2011; Rühs et al., 2015).

Figure 4g shows the southward maximum of the east-west accumulated transports between 15˚S and the equator. The generally good agreement of this interior component of the circulation between the ORAs is in striking contrast with their ψ_{max} (Fig. 2). Indeed the ENS-ORA spread of the interior flow (~1 Sv) is about three time less than the spread in ψ_{max} for the same latitude range. The ORA southward transports differ from the FRMs, with two peaks of southward transport between 10˚S and the equator where the FRMs only have one. The zonal currents, which can be inferred in Fig. 4, reveal consistent changes in the equatorial current system between the ORAs and the FRMs. The central branch of the South Equatorial Current (cSEC), described in the top 500 m tropical circulation schematics of Stramma and Schott (1999) and Talley (2011), is absent in the FRMs, but evident in the ORAs, also leading to stronger southward transports in Fig. 4g. Thus there is both qualitative and quantitative evidence that the DA in the ORAs is doing a good job in reproducing a consistent interior circulation for the tropical South Atlantic basin.

Despite evidence of the ORAs consistency in the interior circulation in the tropical South Atlantic as well as in the subtropical gyre further south, the overturning transport component ψ_{max}, associated with the very narrow NBC, is not as well constrained. Figure 5 shows transports of the NBC at 11˚S, calculated between neutral density interfaces as in Hummels et al. (2015). Although DA brings the ORA NBC transports closer to the observations when compared to the FRMs, the spread is still large.

The UR025.4 and GLORYS2V4 NBC transports have 23.9 ± 1.1 Sv and 25.0 ± 1.3 Sv, quite close to the Schott et al. (2005) and Hummels et al. (2015) observed NBC values of 25.8 ± 1.2 Sv and 26.8 ± 1.8 Sv, respectively. However, the weaker transports in ORAP5 and CGLORSV5 mean that the ENS-ORA spread in the NBC transports is ~3 Sv, which is consistent with the ENS-ORA spread in the SAMOC strength (Fig. 2b). This suggests that, at least in this latitude range, the NBC strength alone can explain the large-scale transport discrepancies between the ORAs, which will be discussed in more detail in Sect. 3.3.

3.2 T and v contributions

In this section, the contributions from T and v variability for the heat transports are analysed, as well as the relationship between the MHT and the SAMOC upper limb. Figure 6 shows a meridional section of the zonal-mean temperatures from WOA13 ~~(Locarnini et al., 2013)~~, together with zonal-time mean anomaly T from each product. Large anomalies in the FRMs can be seen, particularly in the tropics where the models may have limitations representing sharp vertical gradients in the tropical thermocline. In ORCA025, there is a large warm anomaly of up to 3˚C in the upper 200 m of the tropical South Atlantic, whereas ORCA0083 has a weaker warm anomaly in the top 200 m, but a much more extensive cold anomaly of ~2˚C in the ocean interior down to ~500 m. All the ORAs show much weaker anomalies (mostly <0.5˚C), presumably due to the assimilation of SST and T/S profiles which are able to better constrain the T vertical structure. Below 1200 m the differences between the products and WOA13 are much smaller.

Figure 7 evaluates the relative T and v contributions to the ENS-ALL MHT spread. We compare the original MHTs (Fig. 7a) with the MHTs based only on circulation differences ($v\bar{T}$; Fig. 7c), and only on temperature differences ($\bar{v}T$; Fig. 7e), where the overbar denotes the ENS-ALL mean. In order to ~~precisely~~ identify locations where T and v ~~are leading~~contribute to different transports in ENS-ALL, ocean temperature transports per 0.25˚ of longitude (p-OTTs) from top to bottom are also calculated across the basin (Fig. 7b), with their p-$v\bar{T}$ (Fig. 7d) and p-$\bar{v}T$ (Fig. 7f) contributions. Note that the units in the maps of Figs. 7b,d,f are PWT (PetaWatt Temperature Transport; Talley, 2003~~8~~; Macdonald and Baringer, 2013) per 0.25˚. The spatial discretisation of the MHT on a longitudinal 0.25˚ grid allows to present ORCA0083 on a comparable scale to that of the other models.

The strong similarity between Figs. 7a,b and Figs. 7c,d reveals that v rather than T differences drive the inter-product spread in the MHTs, both regionally and in the zonal integrals. The $v\bar{T}$ component captures variations from ~0.2 PW to 1 PW (Fig. 7c), explaining ~83% of the total MHT spread which is mainly concentrated in the areas with largest mean transports, i.e. the narrow western boundary region (Fig. 7d). Even with relatively large T anomalies found in the FRMs (Fig. 6), the $\bar{v}T$ component only differs by ~0.13 PW between the products across the basin (Fig. 7e), mainly due to temperature differences in ORCA025 and ORCA0083. However, a very narrow ~~line~~ maximum of p-$\bar{v}T$ (Fig. 7f) can also be seen right against the western boundary, especially in the NBC region around 11˚S and near the Brazil-Malvinas Confluence at 35˚S. This is interpreted as due to variations in boundary temperatures needed to geostrophically support the large differences in western boundary current velocities between the products~~,~~. However, ~~but~~these temperature differences make ~~it has very~~ little ~~direct T~~ transport contribution. The detailed role of the western boundary for the inter-product transport discrepancies will be discussed again in Sect. 3.3.

The dominance of the circulation determining heat transports also extends to the time variability. The monthly correlation between ψ_{max} and MHT within all products is above 0.8 for most of the South Atlantic (Fig. 8). Dong et al. (2009) and Garzoli et al. (2013) estimated quarterly correlation values around 0.75 between circulation and heat transports at 35˚S from the XBT-AX18 observations. Majumder et al. (2016) found that a 1 Sv change in the SAMOC strength corresponds to a change of 0.046 PW at 35˚S and 0.056 PW at 20˚S in the MHT. This agrees relatively well with the ENS-ORA which show a 1 Sv change in SAMOC strength corresponds to ~0.052 PW change between 35˚S and 20˚S. It is interesting to note that correlations abruptly fall from 0.85 to ~0.45 near the equator. The interior southward flow gradually increases in the tropical South Atlantic reaching similar magnitudes to ψ_{max} between 5˚S and the equator (Fig. 4g). In this region, the temperature differences between the NBC core and the southward basin interior circulation reach up to 5.5˚C in the top 400 m, similar to the ΔT of ~6.5˚C between the SAMOC upper and lower limbs (not shown). Therefore it is likely that these large upper level ~~southward~~ tropical circulations ~~therefore~~ explain why ψ_{max} does not dominate the MHT variability close to the equator, as also noted by Valdivieso et al. (2014).

3.3 Western boundary contribution

Figure 9 shows the linear regression coefficient between the inter-product p-OTTs and their MHTs across the whole basin. The western boundary grid points in the tropical South Atlantic reach up to ~0.4 PWT per 0.25˚, out of 1 PW across the whole basin, so that ~40% of the differences in the MHT can be explained by transports in a 0.25˚-wide band (a single grid point in all models except ORCA0083), with values elsewhere in the basin interior very close to zero. This is consistent with Fig. 4 showing that the large-scale southward flow at upper levels does not differ much between products, while ψ_{max} varies considerably, mainly due to the narrow NBC. Weaker negative linear regression coefficients are found eastward of the NBC in Fig. 9, representing the influence of the southward Deep Western Boundary Current (DWBC), reflecting the sloping bathymetry and the broader current scale than the NBC. South of 25˚S the p-OTT contributions to the total MHT are more distributed ~~across the basin~~, with a noticeable contribution from the Agulhas leakage ~~to the spread.~~ caused by the different intensity and positioning of the Agulhas rings between the products as they travel westward across the Cape basin.

Figure 9 also shows a continuous and dominant narrow band of positive regression coefficients all down the western boundary, including latitudes where the p-OTTs have a southward transport associated with the Brazil Current (BC), e.g. between 35˚S and 25˚S (see schematic of Fig. 1). This reveals that products with larger northward MHTs (e.g. CGLORSV5, UR025.4 and GLORYS2V4) must have weaker southward p-OTTs near the western boundary, i.e. a weaker BC, resulting in the positive MHT linear regressions. In the case of CGLORSV5, UR025.4 and GLORYS2V4, this is reinforced by a stronger northward subsurface transport of the Intermediate Western Boundary Current (IWBC) and North Brazil Undercurrent (NBUC), which feeds the NBC in the tropical South Atlantic (Fig. 10a and Fig. 10b). Based on Fig. 9, a region within 6˚ of the coast is selected to calculate the Tropical Water (TW), South Atlantic Central Water (SACW) and Antarctic Intermediate Water (AAIW) transports of the upper western boundary circulation, with their isopycnal limits defined as in Mémery et al. (2000) and Donners et al. (2005). For each latitude, any southward water mass transport is accounted for as the BC (Fig. 10a), whereas any northward transport contributes to the IWBC-NBUC-NBC system (Fig. 10b), allowing to represent the deepening of the poleward BC and the shallowing of the equatorward IWBC-NBUC-NBC flows, as shown by Fig. 1 (Soutelino et al., 2013).

In GLORYS2V4 and UR025.4, the IWBC and NBUC transports are at least 5 Sv larger than in ORAP5 and the FRMs (Fig. 10b), and the former products then produce a stronger NBC in the tropical South Atlantic, consistent with the observational estimates at 11˚S (Fig. 5). At each latitude the ORAs usually modify the upper western boundary circulation in the same

direction, increasing (decreasing) the transports of the northward (southward) currents compared to the FRMs, which leads to higher MHTs across the entire basin. However, the western boundary transport magnitudes are not properly constrained in the ORAs, as reinforced by Fig. 10c, with the ENS-ORA spread increasing as current strengths increase. The IWBC-NBUC-NBC spread particularly growths from ~1 to 3.5 Sv towards the north which is comparable to the SAMOC spread seen in Fig. 2b. There is much better agreement for the BC near 35˚S between the ORAs (ORAP5 excepted), with spreads smaller compared to the NBC.

In Fig. 11, the transports are schematically broken down into four boxes, the upper and lower western boundary region (within 6° of the coast), and the upper and lower ocean interior (z_{max} separates the upper and lower layers). Figure 11 summarises how the inter-product changes in the upper western boundary circulation correlate with the other three boxes (for the current systems involved see Fig. 1). In the tropical South Atlantic (Fig. 11a), the northward flows in the upper western boundary box in GLORYS2V4 and UR025.4 are ~10 Sv and 8.5 Sv larger than in ORCA025, respectively. These are mainly compensated by larger flows in the DWBC, by ~9 Sv and 8 Sv in GLORYS2V4 and UR025.4, respectively, relative to ORCA025. These large inter-product compensations confined to the western boundary extend to the subtropical region (Fig. 11b), where the ORAs with highest southward DWBC transports show highest northward transports in the western boundary upper limb. Similarly, Sitz et al. (2015) found that the strengthening in the SAMOC upper limb with increasing model resolution is mainly compensated by strengthening of the poleward transport in the deeper layers, mostly in the western part of the basin. This large compensation between the upper and lower western boundary circulation is evident within all products in Fig. 11a, with the deep western boundary typically compensating ~75% of its upper limb transports, which was also noted in observations (Schott et al. 2005; Hummels et al. 2015).

In contrast to their western boundary circulations, the ORAs show very similar upper interior flows across the South Atlantic, consistently stronger than in the FRMs, regardless of direction (southward in Fig. 11a and northward in Fig. 11b). This consistency is retained even in the subtropical gyre (Fig. 11b), where the northward basin interior circulation can have larger magnitude than the upper western boundary currents to balance the DWBC. The deep interior box has negligible transports in the tropical South Atlantic, but significant southward transports further south, especially in the ORAs, suggesting that some portion of the NADW flows towards the interior of the basin in the subtropical South Atlantic (Garzoli et al., 2015).

3.4 Temporal variability

Figures 12a-f show that the interannual variability in p-OTTs is larger in the ORAs and in the high resolution ORCA0083 than in ORCA025. ~~, as also noted by Masina et al (2015).~~ The assimilation of observations in eddy-permitting models introduces variability that would otherwise only appear with higher resolution, as in ORCA0083. According to Masina et al. (2015), this higher variability in the ORAs is in better agreement with the Eddy Kinetic Energy estimates from the ocean surface current velocities (OSCAR) product than that of the FRMs. Although some of the ORAs have more transport variability than others throughout the basin, the western boundary variability remains a dominant feature, particularly northward of 25˚S. In Fig. 12g, the interannual p-OTTs variances for each product are summed within 6˚ of the western boundary coast ~~across each~~as a function of latitude and displayed as a percentage of the total MHT variance~~. Therefore Fig. 12g emphasises~~. It shows that the western boundary controls ~70% of the interannual MHT variability in the tropical South Atlantic for almost all the products (UR025.4 excepted), but it is less dominant further south.

South of ~~this latitude~~25˚S, the interannual variability of the transports is more spread, ~~out across the basin, peaking not only in~~ with contributions from the western boundary (near the Brazil-Malvinas confluence), ~~but also~~ and near the eastern boundary (due to the Agulhas leakage) with the largest values around 0.06 PWT per 0.25˚ in ORCA0083, UR025.4 and GLORYS2V4. The different levels of variability in the Agulhas leakage between ORCA025 and ORAs may be attributed to the impacts of the SLA assimilation (Backeberg et al., 2014). However, even between ORAs these Agulhas patterns differ, e.g. the weaker contributions in ORAP5 may be due to smoothing from the super-observation method applied to the altimeter data (Mogensen et al., 2012), as also noted by Masina et al. (2015). ~~In Fig. 12g, the interannual p-OTTs variances for each product are summed within 6˚ of the west coast across each latitude and displayed as a percentage of the total MHT variance. Therefore Fig. 12g emphasises that the western boundary controls ~70% of the interannual MHT variability in the tropical South Atlantic for almost all the products (UR025.4 excepted), but it is less dominant further south.~~

Figure 13a shows the monthly time series of both ψ_{max} and the maximum southward flow in the basin interior (as in Fig. 4g), as a spatial average from 15˚S to the equator. There appears to be greater consistency in the ORA southward transports in the second half of the time series, which is not seen in ψ_{max}. In Fig. 13b, the time series of the ENS-ORA spread for both

components are also displayed. A running mean of 6 months was applied to smooth the ENS-ORA monthly variability. Even with large variations, particularly in the first years of the time series, the ENS-ORA spread for the upper southward flow is seen to reduce from ~3 Sv to 1 Sv in the later years. This may be explained by the initiation of the Argo program and the increased number of observations to constrain the southward interior flow in the ORAs. The southward interior transports in the ORA maps of Fig.4 from 2008 to 2010 are also more consistent than before 2002, as are their northward interior transports between 30˚S and 15˚S in the later years (not shown). However, the ENS-ORA spread in ψ_{max} remains nearly steady over this period, although the assimilation does increase the NBC transports in the ORAs relative to the FRMs (Fig. 5).

4. Discussion and conclusions

In this work, the South Atlantic meridional transports between 35˚S and the equator were evaluated for a global NEMO-based dataset of four ORAs and two FRMs with distinct spatial resolutions. The ORAs mainly differ by their initial conditions, their DA schemes and to some small extent by the observations assimilated, as they share very similar ocean model configurations and are all forced with the ERA-Interim atmospheric product (Tab. 1).

Some aspects of the circulation are well constrained by data assimilation. The ORA transports in the basin interior are consistently modified across the basin relative to the FRMs (Fig. 4 and Fig. 11), with improvements in the south equatorial currents, and with interior meridional transports converging as Argo data are introduced (Fig. 13). Zonally integrated temperature sections for the ORAs are also very similar to WOA13 (Fig. 6), whereas the FRMs have large anomalies. The relationship between the magnitudes of SAMOC and MHT in the ORAs is in good agreement with that inferred in observations (e.g. Garzoli et al., 2013; Majumder et al., 2016), . ~~The~~and the SAMOC upper limb and MHT are also strongly correlated in time at most latitudes (Fig. 8)~~, except near the equator where a southward basin interior flow contributes to the MHT variability~~.

The DA does appear to systematically increase the ORA SAMOCs and MHTs with respect to the FRMs, bringing them closer to observational estimates at 35˚S and western boundary measurements at 11˚S (Fig. 3 and Fig. 5). The assimilation of Argo data, for example, leads to a significant intensification of the boundary currents relative to the pre-Argo period and to an improvement in the SAMOC structure at 35˚S in comparison with XBT-AX18 estimates (see also Dong et al. (2011a)). Here, although the DA ~~mostly~~ consistently changes the upper western boundary transports in the same direction (e.g. increasing the

northward IWBC-NBUC-NBC and decreasing the southward BC), they do not consistently constrain the boundary current transport magnitudes. ~~Therefore, l~~Large SAMOC and MHT discrepancies still remain between the ORAs. These discrepancies~~, which~~ are mainly attributed to differences in the narrow South Atlantic western boundary currents found within a few degrees of the coast. For example, the NBC (15˚S-equator) explains ~85% of the inter-product differences in the total MHTs, with compensating variations in the return flow (DWBC) also close to the coast. Since the overturning stream function ψ_{max} is mainly associated with these boundary flows, it is not well constrained by the ORAs, particularly in the tropical South Atlantic.

Analysis of the heat transports also reveals that differences in transport rather than differences in temperature dominate the inter-product spread, even within the western boundary region. The temperature contribution to the inter-product spread in heat transport, $\bar{v}T$, is only ~17% of the total spread, but its signature is evident right against the western boundary where temperature differences are required to geostrophically support the velocity differences between products. The local response to small density changes on the western boundary slope was also found to largely determine the meridional transport variability in ocean models in the North Atlantic, as noted by Bingham and Hughes (2009), emphasising the large sensitivity of the currents with respect to local density gradients against the boundary.

It is noteworthy that the lateral boundary conditions in the ORAs and FRMs vary between free-slip (α=0) and partial-slip (α=0.5). However, there is no clear correspondence between the choice of lateral boundary conditions and the strength of the western boundary transports, with free-slip products (e.g. UR025.4) having similar transports to partial-slip products (e.g. GLORYS2V4).

Two possible reasons for the ORA differences in the western boundary currents are: (i) the lack of near boundary observations, and/or (ii) the differences in DA error covariances when assimilating interior basin measurements lying near to the western boundary. Observation system simulation experiments (OSSEs) with AMOC trans-basin arrays have shown that the meridional flow strength can be sensitive to the number of hydrographic profiles near the boundaries in both North (e.g. Hirschi et al., 2003; Baehr et al., 2004) and South Atlantic (e.g. Perez et al., 2011). The combined assimilation of open ocean hydrographic observations and ~~with~~ the ~~-~~continuous RAPID array western boundary measurements ha~~s~~ves ~~already~~ also been ~~demonstrated~~ shown to locally improve the AMOC ~~structure~~ strength at 26.5˚N ~~, with positive impacts also extending to higher and lower latitudes~~ (Stepanov et al., 2012). This emphasises the role that more systematic observations located at the eastern and western

boundaries at several latitudes may play in monitoring the AMOC (Marotzke et al., 1999). In the future, the SAMOC observing system (Ansorge et al., 2014; Hummels et al., 2015), which will provide time series of NBC measurements at the western boundary at 11˚S, could be assimilated into the ORAs to constrain the regions of largest spread in the tropical South Atlantic.~~A similar approach may in future be possible for the South Atlantic, particularly for the regions of largest spread in the tropical South Atlantic, where the SAMOC observing system (Ansorge et al., 2014; Hummels et al., 2015) will provide time series of NBC measurements at the western boundary at 11˚S.~~

Differences in data assimilation methods near ~~to~~ the boundaries may also be influencing the overturning in the different ORAs. For example, Balmaseda et al. (2013) noted that the AMOC at 26˚N in the ECMWF reanalyses is very sensitive to the treatment of observations and the parametrization of their errors near to the boundaries, although similar changes are not documented for other ORAs. Stepanov et al. (2012) also showed that the assimilation impacts of the RAPID western boundary measurements on the AMOC can vary according to the prescribed horizontal scales of the DA error covariances, e.g. with boundary-focused covariances producing larger positive impacts on the AMOC than isotropic covariances. ~~For this reason, in~~In order to better understand the large SAMOC sensitivity found between the ORAs, future work ~~should~~ will focus on the response of the western boundary and SAMOC transports to changes in the ORA configurations, such as sensitivity experiments to the assimilated datasets and to the DA schemes near to the western boundary.

Acknowledgments. The first author would like to acknowledge the financial support of the CAPES Foundation, Ministry of Education of Brazil (Proc. BEX 1386/15-8). The authors also would like to mention the support of the ORA providers and the Copernicus Marine Service (http://marine.copernicus.eu/) to provide access of the reanalysis data used in this work.

References

Adcroft, A., Hill, C., and Marshall, J.: Representation of topography by shaved cells in a height coordinate ocean model, Mon. Weather Rev., 125, 2293–2315, 1997.

Ansorge, I. J., Baringer, M. O., Campos, E. J. D., Dong, S., Fine, R. A., Garzoli, S. L., Goni, G., Meinen, C. S., Perez, R. C., Piola, A. R., Roberts, M. J., Speich, S., Sprintall, J., Terre, T., and Van den Berg, M. A.: Basin-Wide Oceanographic Array Bridges the South Atlantic, Eos, 95, 53-54, 2014.

Backeberg, B. C., Counillon, F., Johannessen, J. A., and Pujol, M.-I.: Assimilating along-track SLA data using the EnOI in an eddy resolving model of the Agulhas system, Ocean. Dynam., 64, 1121-1136, doi: 10.1007/s10236-014-0717-6, 2014.

Baehr, J., Hirschi, J., Beismann, J.-O., and Marotzke, J.: Monitoring the meridional overturning circulation in the North Atlantic: A model-based array design study, J. Mar. Res., 62, 283-312, 2004.

Balmaseda, M. A., Mogensen, K., and Weaver, A. T.: Evaluation of the ECMWF ocean reanalysis system ORAS4, Q. J. Roy. Meteror. Soc., 139, 1132-1161, 2013.

Balmaseda, M.A., Hernandez, F., Storto, A., Palmer, M. D., Alves, O., Shi, L., Smith, G. C., Toyoda, T., Valdivieso, M., Barnier, B., Behringer, D., Boyer, T., Chang, Y-S., Chepurin, G. A., Ferry, N., Forget, G., Fujii, Y., Good, S., Guinehut, S., Haines, K., Ishikawa, Y., Keeley, S., Kohl, A, Lee, T., Martin, M. J., Masina, S., Masuda, S., Meyssignac, B., Mogensen, K., Parent, L., Peterson, K. A., Tang, Y. M., Yin, Y., Vernieres, G., Wang, X., Waters, J., Wedd, R., Wang, O., Xue, Y., Chevallier, M., Lemieux, J-F., Dupont, F., Kuragano, T., Kamachi, M., Awaji, T., Caltabiano, A., Wilmer-Becker, K., and Gaillard, F.: The Ocean Reanalyses Intercomparison Project (ORA-IP), J. Oper. Oceanogr., 8, 80-97, 2015.

Barnier, B., Madec, G., Penduff, T., Molines, J. M., Treguier, A. M., Le Sommer, J., Beckmann, A., Biastoch, A., B¨oning, C., Dengg, J., Derval, J., Durand, E., Gulev, S., Remy, E., Talandier, C., Theetten, S., Maltrud, M., McClean, J., and de Cuevas, B.: Impact of partial steps and momentum advection schemes in a global ocean circulation model at eddy-permitting resolution, Ocean Dynam., 56, 6543–567, doi:10.1007/s10236-006-0082, 2006.

Bingham, R. J., and Hughes, C. W.: Geostrophic dynamics of meridional transport variability in the subpolar North Atlantic, J. Geophys. Res., 114, doi:10.1029/2009JC005492, 2009.

Brodeau, L., Barnier, B., Treguier, A-M., Penduff, T., and Gulev, S: An ERA40- based atmospheric forcing for global ocean circulation models, Ocean Model., 31, 88-104, 2010.

Bryden, H. L., and S. Imawaki: Ocean heat transport, in Ocean Circulation and Climate, edited by G. Siedler, J. Church, and J. Gould, chap. 6.2, pp. 455–474, Academic Press, London, 2001.

Copernicus Marine Environmental Monitoring Service (CMEMS): Product user manual, available at http://marine.copernicus.eu/documents/PUM/CMEMS-GLO-PUM-001-025.pdf, 25 pp., 2017.

Cunningham, S. A., Kanzow, T., Rayner, D., Baringer, M. O., Johns, W. E., Marotzke, J., Longworth, H. R., Grant, E. M., Hirschi, J. J.-M., Beal, L. M., Meinen, C. S., and Bryden H. L.: Temporal Variability of the Atlantic Meridional Overturning Circulation at 26.5˚N, Science, 317, 935-937, 2007.

Dong, S., Garzoli, S., Baringer, M., Meinen, C., and Goni, G.: Interannual variations in the Atlantic meridional overturning circulation and its relationship with the net northward heat transport in the South Atlantic, 36, doi:10.1029/2009GL039356, 2009.

Dong, S., Baringer, M., Goni, G., Meinen, C., and Garzoli, S.: Importance of the assimilation of Argo float measurements on the Meridional Overturning Circulation in the South Atlantic, Geophys. Res. Lett., 38, doi:10.1029/2011GL048982, 2011a.

Dong, S., Garzoli, S., and Baringer, M.: The Role of Interocean Exchanges on Decadal Variations of the Meridional Heat Transport in the South Atlantic, J. Phys. Oceanogr., 41, 1498-1511, 2011b.

Dong, S., Baringer, M., Goni, G., Meinen, C., and Garzoli, S.: Seasonal variations in the South Alantic Meridional Overturning Circulation from observations and numerical models, Geophys. Res. Lett., doi:10.1002/2014GL060428, 2014.

Dong, S., Goni, G., and Bringas, F.: Temporal variability of the South Atlantic Meridional Overturning Circulation between 20˚S and 35˚S, Geophys. Res. Lett., doi: 10.1002/2015GL065603, 2015.

Donners, J., Drijfhout, S. S., and Hazeleger, W.: Water Mass Transformation and Subduction in the South Atlantic, J. Phys. Oceanogr., 35, 1841-1860, 2005.

Drijfhout, S. S.,Weber, S. L., and van der Swaluw, E.: The stability of the MOC as diagnosed from model projections for pre-industrial, present and future climates, Clim. Dynam., doi:10.1007/s00382-010-0930-z, 2011.

Ganachaud, A., and Wunsch, C.: Large scale ocean heat and freshwater transports during the World Ocean Circulation Experiment, J. Climate, 16, 695-705, 2003.

Garric, G., and Verbprugge, N.: Large scale ECMWF radiative surface fluxes assessment, correction and application to 3D global ocean simulations, Geophysical Research Abstracts, vol. 12 EUGU2010-12044, EGU General Assembly, 2010.

Garzoli, S. L., and Baringer, M. O.: Meridional heat transport determined with expandable bathythermographs - Part II: South Atlantic transport, Deep-Sea Res. I, 54, 1402-1420, 2007.

Garzoli, S. L, and Matano, R.: The South Atlantic and the Atlantic Meridional Overturning Circulation, Deep-Sea Res. II, 58, 1837-1847, 2011.

Garzoli, S. L., Baringer, M. O., Dong, S., and Perez, R., and Yao, Q.: South Atlantic Meridional Fluxes, Deep-Sea Res. I, 71, 21-32, 2013.

Garzoli, S. L., Dong, S., Fine, R., Meinen, C., Perez, R. C., Schmid, C., Sebille, E., and Yao, Q.: The fate of the Deep Western Boundary Current in the South Atlantic, Deep-Sea Res. I, 103, 125–136, doi:10.1016/j.dsr.2015.05.008, 2015.

Good, S. A., Martin, M. J., and Rayner, N. A.: EN4: quality controlled ocean temperature and salinity profiles and monthly objective analyses with uncertainty estimates, J. Geophys. Res., 118, 6704–6716, doi:10.1002/2013JC009067, 2013.

Haines, K., Valdivieso, M., Zuo, H., and Stepanov, V. N.: Transports and budgets in a 1/4˚ global ocean reanalysis 1989–2010, Ocean Sci., 8, 333–344, doi:10.5194/os-8–333-2012, 2012.

Hawkins, E., Smith, R. S., Allison, L. C., Gregory, J. M., Woolings, T. J., Pohlmann, H., and de Cuevas, B.: Bistability of the Atlantic overturning circulation in a global climate model and links to ocean freshwater transport, Geophys. Res. Lett., 38, 3L10605, doi:10.1029/2011GL047208, 2011.

Hirschi, J., Baehr, J., Marotzke, J., Stark, J., Cunningham, S., and Beismann J.-O.: A monitoring design for the Atlantic meridional overturning circulation, Geophys. Res. Lett., 30, doi: 10.1029/2002GL016776, 2003.

Hummels, R., Brandt, P., Dengler, M., Fischer, J., Araujo, M., Veleda, D., and Durgadoo, J. V.: Interannual to decadal changes in the western boundary circulation in the Atlantic at 11˚S, Geophys. Res. Lett., 42, doi:10.1002/2015GL065254, 2015.

Janssen, P., Breivik, O., Mogensen, K., Vitart, F., Balmaseda, M., Bidlot, J.-R., Keeley, S., Leutbecher, M., Magnusson, L., and Molteni, F.: Air-sea interaction and surface waves, Technical Report 712 (internal), ECMWF, 2013.

Karspeck, A. R., Stammer, D., Kohl, A., Danabasoglu, G., Balmaseda, M., Smith, D. M., Fujii, Y., Zhang, S., Giese, B., Tsujino, H., and Rosati, A.: Comparison of the Atlantic meridional overturning circulation between 1960 and 2007 in six ocean reanalysis products. Clim. Dynam., doi:10.1007/s00382-015-2787-7, 2015.

Large, W. G. and Yeager, S. G.: Diurnal to decadal global forcing for ocean and sea-ice models: The data sets and flux climatologies, Technical Report TN-460+STR, NCAR, 105 pp., 2004.

Large, W.G. and Yeager, S. G.: The global climatology of an interannually varying air-sea flux data set. Clim. Dynam., 33, 341-364, doi:10.1007/s00382-008-0441-3, 2009.

Levitus, S., Boyer, T. P., Conkright, M. E., O'Brien, T., Antonov, J., Stephens, C., Stathoplos, L., Johnson, D., and Gelfeld, R.: NOAA Atlas NESDIS 18, World Ocean Database 1998: VOUME 1: INTRODUCTION, U.S. Gov. Printing Office, Washington D.C., 346 pp., 1998.

Liu, C., Allan, R. P., Berrisford, P., Mayer, M., Hyder, P., Loeb, N., Smith, D., and Edwards, J. M.: Combining satellite observations and reanalysis energy transports to estimate global net surface energy fluxes 1985-2012, J. Geophys. Res-Atmos., 120, 9374–9389, doi: 10.1002/2015JDO23264, 2015.

Locarnini, R., Mishonov, A., Antonov, J., Boyer, T., Garcia, H., Baranova, O., Zweng, M., and Johnson, D.: World Ocean Atlas 2009, volume 1: Temperature. In: Levitus S (ed) NOAA Atlas NESDIS 68, 184 pp., 2010.

Locarnini, R. A., Mishonov, A. V., Antonov, J. I., Boyer, T. P., Garcia, H. E., Baranova, O. K., Zweng, M. M., Paver, C. R., Reagan, J. R., Johnson, D. R., Hamilton, M., and Seidov, D.: World Ocean Atlas 2013, volume 1: Temperature. In: Levitus S. (ed) NOAA Atlas NESDIS 73, 40 pp., 2013.

Lopez, H., Dong, S., Lee, S., and Goni, G.: Decadal Modulations of Interhemispheric Global Atmospheric Circulations and Monsoons by the South Atlantic Meridional Overturning Circulation, J. Climate, 29, 1831-1851, 2016.

Lumpkin, R. and Speer, K.: Global Ocean Meridional Overturning, J. Phys. Oceanogr., 37, 2550–2562, doi:10.1175/JPO3130.1, 2007.

Macdonald, A. M., and Baringer M. O.: Ocean heat transport, in Ocean Circulation and Climate, edited by Siedler, G., Griffies, S. M., Gould, J., and Church, J. A., chap. 29, 759-786, Academic Press, London, 2013.

Madec, G., and Imbard, M.: A global ocean mesh to overcome the North Pole singularity, Clim. Dynam., 12, 381-388, 1996.

Madec, G.: NEMO ocean engine, Note du Pole de modélisation, Institut Pierre-Simon Laplace (IPSL), France, 27, 1288–1619, 2008.

Majumder, S., Schmid, C., and Halliwell, G.: An observations and model-based analysis of meridional transports in the South Atlantic, J. Geophys. Res-Oceans, 121, doi:10.1002/2016JC011693, 2016.

Marotzke, J., Giering, R., Zhang, K. Q., Stammer, D., Hill, C., and Lee, T.: Construction of the adjoint MIT ocean general circulation model and application to Atlantic heat transport sensitivity, J. Geophys. Res., 104, 529-547, 1999.

Marshall, J., Donohoe, A., Ferreira, D., and McGee, D.: The ocean's role in setting the mean position of the Inter-Tropical Convergence Zone, Clim. Dynam., 42, 1967-1979, 2013.

Marzocchi, A., Hirschi, J. J.-M., Holliday, N. P., Cunningham, S. A., Blaker, A. T., and Coward, A. C.: The North Atlantic subpolar circulation in an eddy-resolving global ocean model, J. Marine Syst., 142, 126-143, 2015.

Masina, S., Storto, A., Ferry, N., Valdivieso, M., Haines, K., Balmaseda, M., Zuo, H., Drevillon, M., and Parent, L: An ensemble of eddy-permitting global ocean reanalyses from the MyOcean project, Clim. Dynam., doi: 10.1007/s00382-015-2728-5, 2015.

Mémery, L., Arhan, M., Alvarez-Salgado, X. A., Messias, M-J., Mercier, H., Castro, C. G., and Rios, A. F.: The water masses along the western boundary of the south and equatorial Atlantic, Prog. Oceanogr., 47, 69-98, 2000.

Mogensen, K., Balmaseda, M. A., and Weaver, A.: The NEMOVAR ocean data assimilation system as implemented in the ECMWF ocean analysis for system 4, Technical Report 668 (internal), ECMWF, 2012.

Palmer, M. D., Roberts, C. D., Balmaseda, M., Chang, Y.-S., Chepurin, G., Ferry, N., Fujii, Y., Good, S. A., Guinehut, S., Haines, K., Hernandez, F., Köhl, A., Lee, T., Martin, M. J., Masina, S., Masuda, S., Peterson, K. A., Storto, A., Toyoda, T., Valdivieso, M., Vernieres, G., Wang, O., and Xue, Y.: Ocean heat content variability and change in an ensemble of ocean reanalyses, Clim. Dynam., doi: 10.1007/s00382-015-2801-0, 2015.

Penduff, T., Le Sommer, J., Barnier, B., Treguier, A.-M., Molines, J.-M., and Madec, G.: Influence of numerical schemes on current-topography interactions in 1/4˚ global ocean simulations, Ocean Sci., 3, 509–524, doi:10.5194/os-3-509-2007, 2007.

Penduff, T., Juza, M., Brodeau, L., Smith, G. C., Barnier, B., Molines, J.-M., Treguier, A.-M., and Madec, G.: Impact of global ocean model resolution on sea-level variability with emphasis on interannual time scales, Ocean Sci., 6, 269–284, doi:10.5194/os- 6-269-2010, 2010.

Perez, R. C., Garzoli, S. L., Meinen, C. S., and Matano R. P.: Geostrophic Velocity Measurement Techniques for the Meridional Overturning Circulation and Meridional Heat Transport in the South Atlantic, J. Atmos. Ocean. Tech., 28, 1504-1520, 2011.

Pham, D. T., Verron, J., Roubaud, and Roubaud, M. C.: A singular evolutive extended Kalman filter for data assimilation in oceanography, J. Marine Syst., 16, 323-340, 1998.

Rabe, B., Schott, F. A., and Köhl, A.: Mean circulation and variability of the tropical Atlantic during 1952-2001 in the GECCO assimilation fields, J. Phys. Oceanogr., 38, 177-192, 2008. Rühs, S., Getzlaff, K., Durgadoo, J. V., Biastoch, A., and Böning, C. W.: On the suitability of North Brazil Current transport estimates for monitoring basin-scale AMOC changes, Geophys. Res. Lett., 42, 8072–8080, doi:10.1002/2015GL065695, 2015.

Rühs, S., Getzlaff, K., Durgadoo, J. V., Biastoch, A., and Böning, C. W.: On the suitability of North Brazil Current transport estimates for monitoring basin-scale AMOC changes, Geophys. Res. Lett., 42, 8072–8080, doi:10.1002/2015GL065695, 2015.

Schott, F. A., Dengler, M., Zantopp, R., Stramma, L., Fischer, J., and Brandt, P.: The shallow and deep western boundary circulation of the South Atlantic at 5˚-11˚S, J. Phys. Oceanogr., 35, 2031-2053, 2005.

Sebille, E. V., Beal, L. M., and Johns, W. E.: Advective Time Scales of Agulhas Leakage to the North Atlantic in Surface Drifter Observations and the 3D OFES Model, J. Phys. Oceanogr., 41, 1026-1034, 2011.

Simmons, A., Uppala S., Dee, D., and Kobayashi, S.: ERA-Interim: New ECMWF reanalysis products from 1989 onwards, ECMWF Newsletter, 110, 25–35, 2007.

Sitz, L. E., Farneti, R., and Griffies, S. M.: Simulated South Atlantic transports and their variability during 1958-2007, Ocean Model., 91, 70-90, 2015.

Smith, G. C., and Haines, K.: Evaluation of the S(T) assimilation method with the Argo dataset, Q. J. Roy. Meteorol. Soc., 135, 739–756, 2009.

Soutelino, R. G., Gangopadhyay, A., and da Silveira, I. C. A.: The roles of vertical shear and topography on the eddy formation near the site of origin of the Brazil Current, Cont. Shelf Res., 70, 46-60, 2013.

Stepanov, V. N., and Haines, K.: Mechanisms for AMOC variability simulated by the NEMO model, Ocean Sci., 10, 645-656, doi: 10.5194/os-10-645-2014, 2014.

Stepanov, V., Haines, K., and Smith, G. C.: Assimilation of Rapid Array data into an ocean model, Q. J. Roy. Meteror. Soc., 138, 2105-2117, 2012.

Stepanov, V. N., Iovino, D., Masina, S., Storto, A., and Cipollone, A.: The impact of horizontal resolution of density field on the calculation of the Atlantic meridional overturning circulation at 34˚S, J. Geophys. Res-Oceans, 121, doi:10.1002/2015JC011505, 2016.

Storkey, D., Blockley, E. W., Furner, R., Guiavarc'h, C., Lea, D., Martin, M. J., Barciela, R. M., Hines, A., Hyder, P., and Siddorn, J. R.: Forecasting the ocean state using NEMO: The new FOAM system, J. Oper. Oceanogr., 3, 3-15, 2010.

Storto, A., and Masina, S.: C-GLORSv5: an improved multipurpose global ocean eddy-permitting physical reanalysis, Earth Syst. Sci. Data, 8, 679-696, 2016.

Storto, A., Dobricic, S., Masina, S., and Di Pietro, P.: Assimilating along-track altimetric observations through local hydro static adjustments in a global ocean reanalysis system, Mon. Weather Rev., 139, 738-754, 2011.

Stramma, L., and Schott, F.: The mean flow field of the tropical Atlantic Ocean, Deep-Sea Res. II, 46, 279-303, 1999.

Talley, L. D.: Shallow, intermediate and deep overturning components of the global heat budget, J. Phys. Oceanogr., 33, 530–560, 2003.

Talley, L. D.: Freshwater transport estimates and the global overturning circulation: Shallow, deep and throughflow components, Prog. Oceanogr., 78, 257–303, 2008.

Talley, L.D., Pickard, G.L., Emery, W.J., and Swift, J.H.: Descriptive Physical Oceanography: An Introduction (Sixth Edition), Elsevier, Boston, 560 pp, 2011.

Timmermann, R., Goosse, H., Madec, G., Fichefet, T., Ethe, C., and Duliere, V.: On the representation of high latitude processes in the ORCA-LIM global coupled sea ice-ocean model, Ocean Model., 8, 175–201, 2005.

Treguier, A. M., Deshayes, J., Le Sommer, J., Lique, C., Madec, G., Penduff, T., Molines, J.-M., Barnier, B., Bourdalle-Badie, R., and Talandier, C.: Meridional transport of salt in the global ocean from an eddy-resolving model, Ocean Sci., 10, 243-255, 2014.

Trenberth, K. E., and Caron, J. M.: Estimates of meridional atmosphere and ocean heat transports, J. Climate, 14, 3433-3443, 2001.

Valdivieso, M., Haines , K., Zuo, H., and Lea, D.: Freshwater and heat transports from global ocean synthesis, J. Geophys. Res-Oceans, 119, 394-409, doi:10.1002/2013JC009357, 2014.

Weijer, W., de Ruijter, W. P. M., Sterl, A., and Drijfhout, S. S.: Response of the Atlantic overturning circulation to South Atlantic sources of buoyancy, Global Planet. Change, 34, 293-311, 2002.

Zuo, H., Mugford, R. I., Haines, K., and Smith, G. C.: Assimilation impacts on Arctic Ocean circulation, heat and freshwater, Ocean Model., 40, 147–163, doi:10.1016/j.ocemod.2011.08.008, 2011.

Zuo, H., Balmaseda, M. A., and Mogensen, K.: The new eddy-permitting ORAP5 ocean reanalysis: description, evaluation and uncertainties in climate signals, Clim. Dynam., doi: 10.1007/s00382-015-2675-1, 2015.

Tables

Table 1. List of the NEMO-based products used in this study and their central characteristics. Abbreviations: OSTIA stands for Operational Sea Surface Temperature and Sea Ice Analysis, AVISO for Archiving, Validation and Interpretation of Satellites Oceanography, AVHRR for Advanced Very High Resolution Radiometer, AMSR-E for Advanced Microwave Scanning Radiometer for Earth Observing System, NSIDC for National Snow and Ice Data Center, ICOADS for International Comprehensive Ocean-Atmosphere Data Set, NODC for National Oceanographic Data Center, EUMETSAT for European Organisation for the Exploitation of Meteorological Satellites, OSISAF for Ocean and Sea Ice Satellite Application Facility, CORA for Coriolis Dataset for Re-Analysis, and CERSAT for Centre ERS d'Archivage et de Traitement.

Product	Model / Resolution	Atmospheric Forcing	Data assimilation	Assimilated observations	Initial conditions
ORCA025	NEMO3.2 – LIM2, 1/4˚, 46 z-levels	6-hourly ERA-Interim	None	None	1/4˚ run with hydrographic data assimilation
ORCA0083	NEMO3.2 – LIM2, 1/12˚, 75 z-levels	6-hourly DFS4.1 (1978 -2007) and 5.1 (2008-2010)	None	None	Levitus (1998) T/S climatology
ORAP5	NEMO3.4.1 – LIM2, 1/4˚, 75 z-levels	6-hourly ERA-Interim with wave forcing	NEMOVAR (3D-Var) (Mogensen et al., 2012)	OSTIA SST, AVISO SLA, in situ T/S profiles from EN3_v2 with bias correction for XBT, OSTIA sea-ice concentration	12-year spin-up initialised from WOA09 T/S climatology and followed by 5-year assimilation run
CGLORSV5	NEMO3.2.1 – LIM2, 1/4˚, 50 z-levels	3-hourly ERA-Interim	Global OceanVar (3D-Var) (Storto et al., 2011)	Reynolds 1/4˚ AVHRR + AMSR-E SST, AVISO SLA, in situ T/S profiles from EN3_v2 with bias correction for XBT, NSIDC ("NASA Team" algorithm) sea ice concentration	Mean January condition of a 4-year spin-up initialised from EN4 T/S analysis
UR025.4	NEMO3.2 – LIM2, 1/4˚, 75 z-levels	6-hourly ERA-Interim	Met Office FOAM – NEMO assimilation system (Optimal Interpolation) (Storkey et al., 2010)	ICOADS in situ SST and NODC satellite SST, AVISO SLA, in situ T/S profiles from EN3_v2 with bias correction for XBT, EUMETSAT OSISAF sea ice concentration	EN3 T/S analysis
GLORYS2V4	NEMO3.1 – LIM2, 1/4˚, 75 z-levels	3-hourly ERA-Interim with RF and P corrections	SAM2 (Singular Evolutive Extended Kalman Filter) (Pham et al., 1998)	Reynolds 1/4˚ AVHRR-only SST, AVISO SLA, in situ T/S profiles from Coriolis CORA4.1 database, CERSAT sea ice concentration	EN4 T/S analysis

Figures

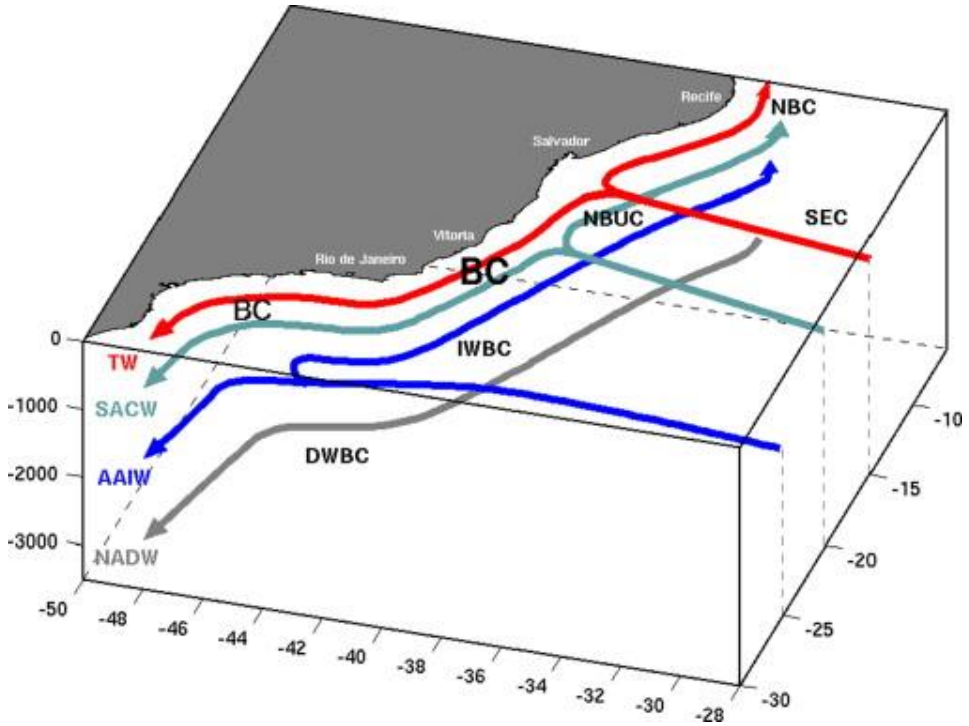

Figure 1. 3D schematic of the South Atlantic western boundary circulation and water masses from Soutelino et al. (2013). The water masses associated with the SAMOC upper limb are represented by the Tropical Water (TW), South Atlantic Central Water (SACW) and Antarctic Intermediate Water (AAIW). The circulation is represented by the Brazil Current (BC), Intermediate Western Boundary Current (IWBC), North Brazil Undercurrent (NBUC), North Brazil Current (NBC) and South Equatorial Current (SEC). The Deep Western Boundary Current (DWBC) is also shown flowing poleward along the NADW path.

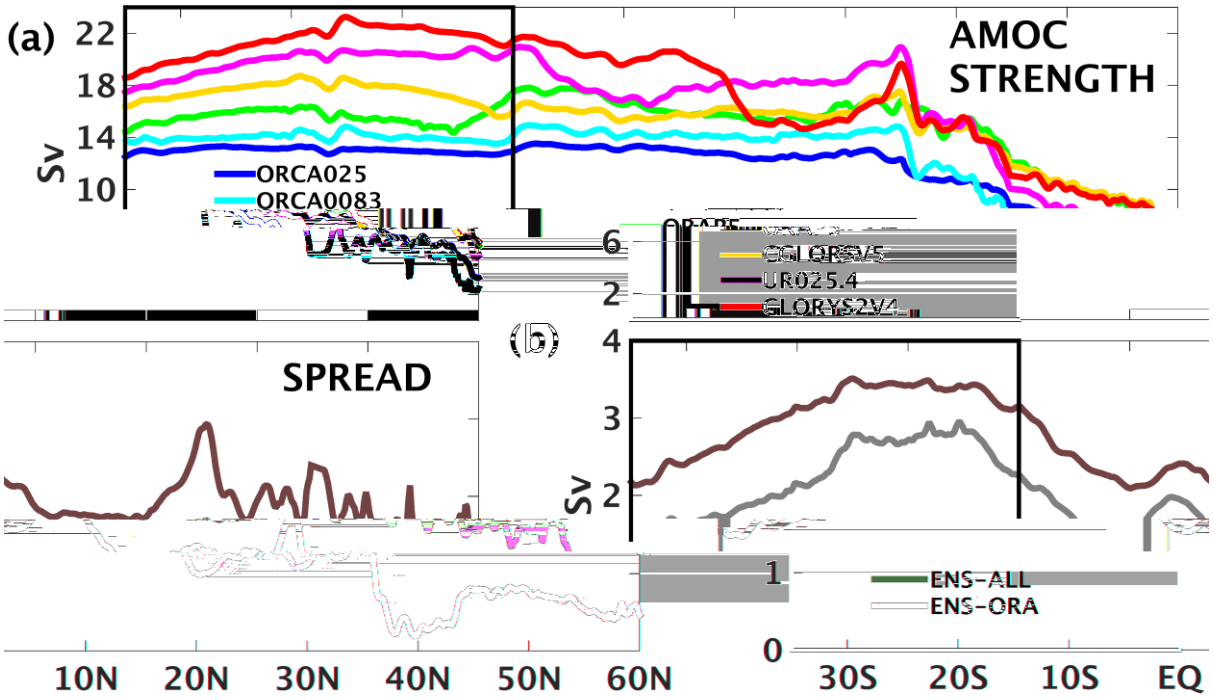

630

Figure 2. (a) The AMOC strength ψ_{max} (Sv) averaged over 1997-2010 as a function of latitude, and (b) its spread (Sv) defined as the standard deviation of ~~for~~ the ENS-ALL and ENS-ORA. The black box represents the study area between 35˚S and the equator.

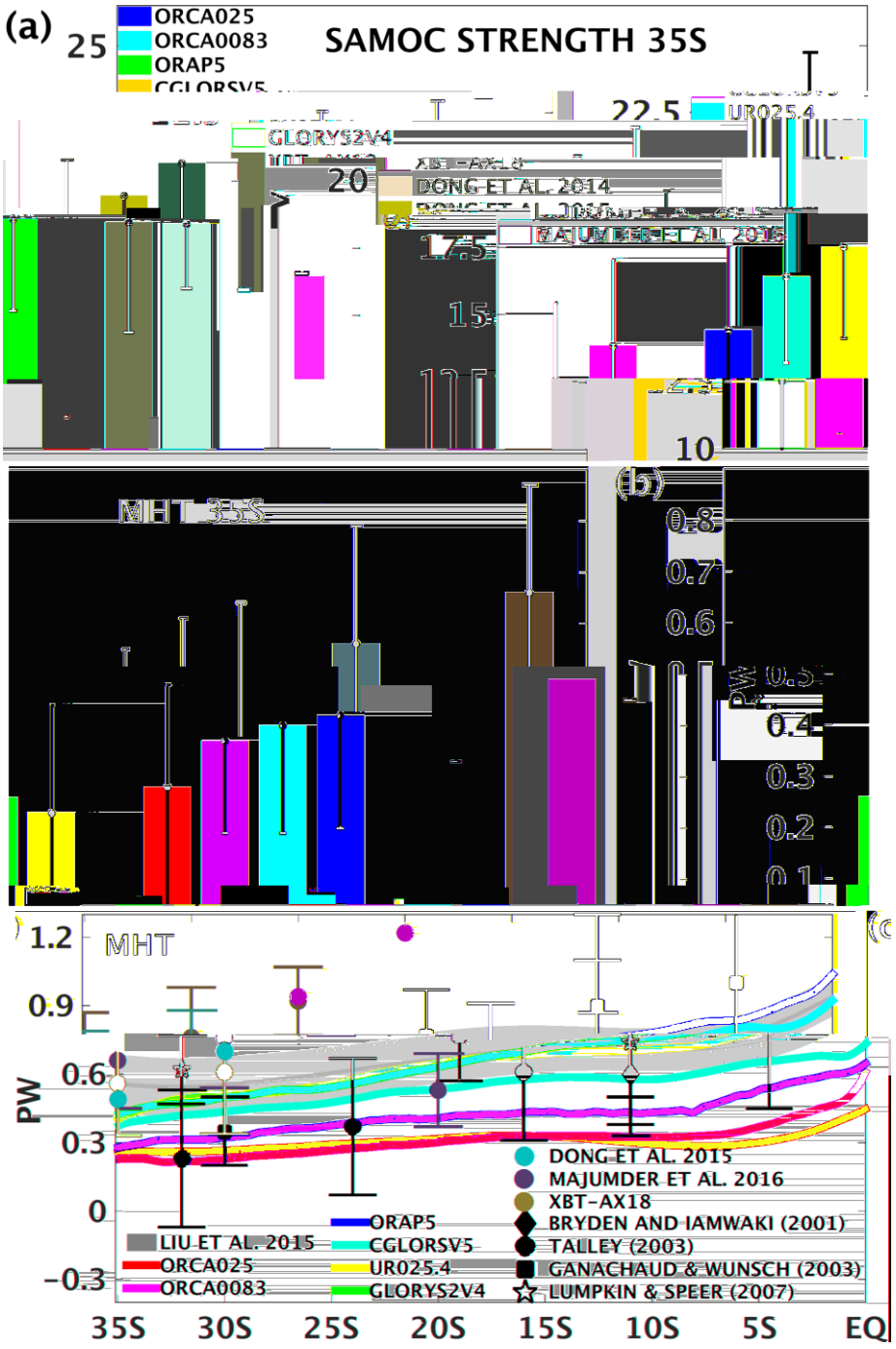

Figure 3. (a) SAMOC strength (Sv) at 35˚S, (b) MHT (PW) at 35˚S, and (c) MHT (PW) as a function of latitude averaged over 1997-2010. The black bars in (a) and (b) represent monthly standard deviations, except for the XBT-AX18, Dong et al. (2015) and Majumder et al. (2016) estimates which correspond to quarterly, weekly and daily standard deviations, respectively. In (c), Liu et al. (2015)'s MHTs and their annual standard deviation are represented by the shaded grey area. The products are also compared to hydrographic and inverse modelling estimates from the literature at several latitudes.

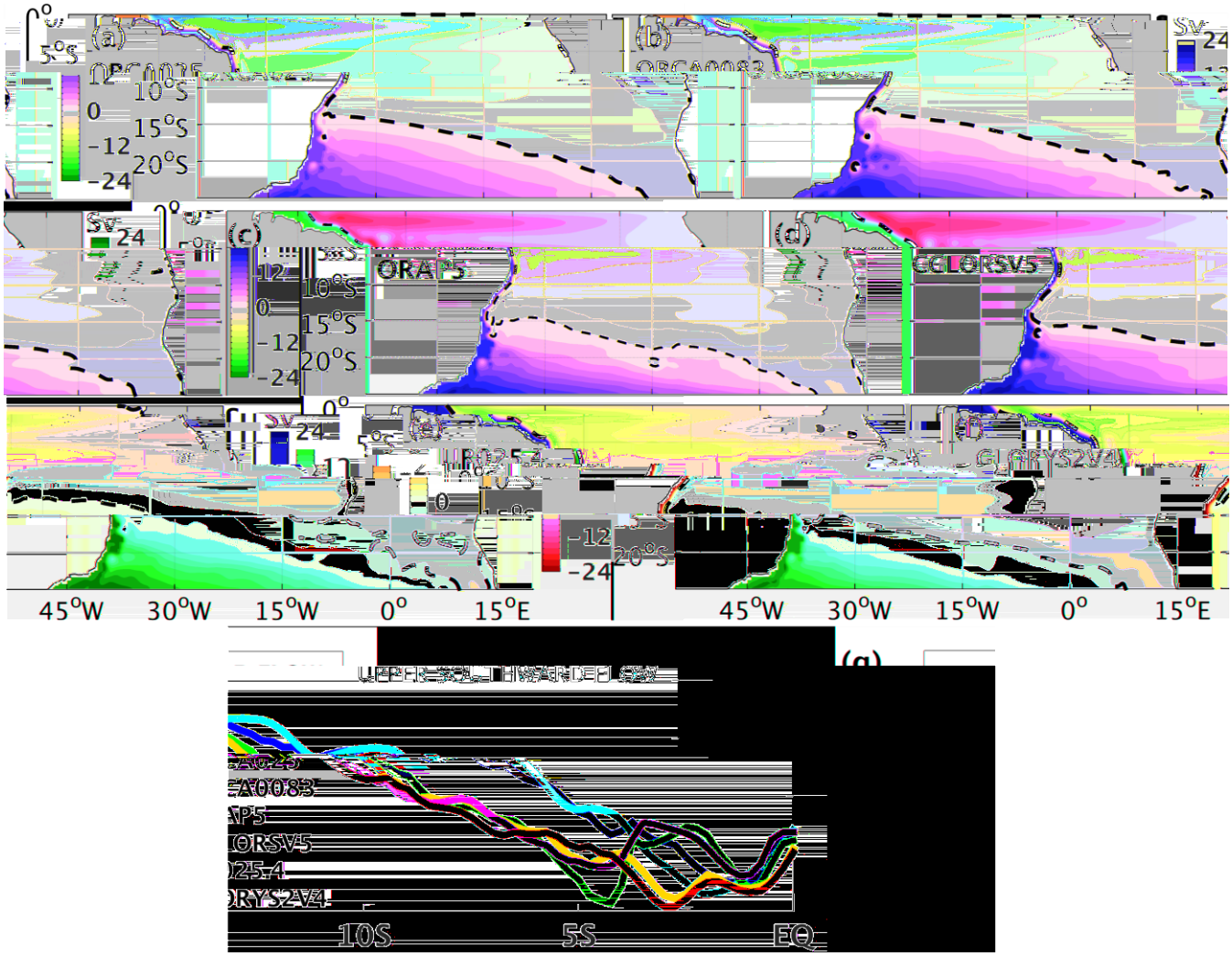

Figure 4. East-west accumulated volume transports (1997-2010) for each product (a to f) calculated from the surface down to z_{max} at each latitude. The upper southward flow in (g) is defined by the southward maximum of the east-west accumulated volume transports. Units are in Sv and the black dashed contour corresponds to 0 Sv.

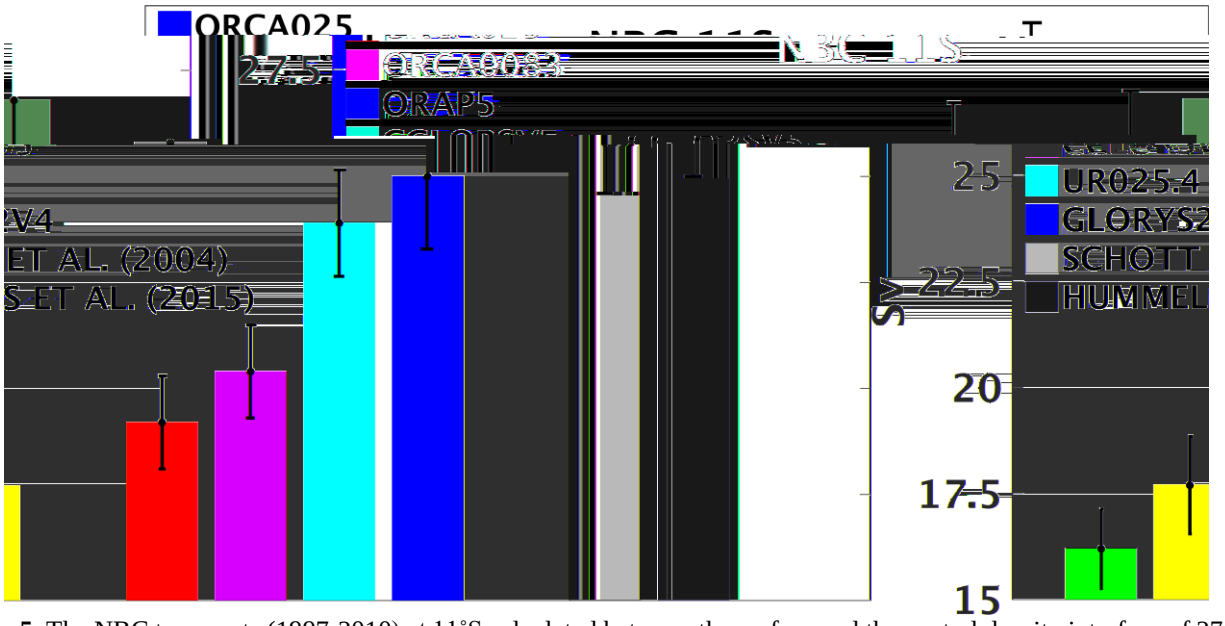

Figure 5. The NBC transports (1997-2010) at 11˚S calculated between the surface and the neutral density interface of 27.7 kg m^{-3}, using the same section near the western boundary and methodology as in Hummels et al. (2015). The black bars represent the standard errors where the size of the sample is defined as the length of the monthly time series. ~~and the~~ U~~u~~nits are in Sv.

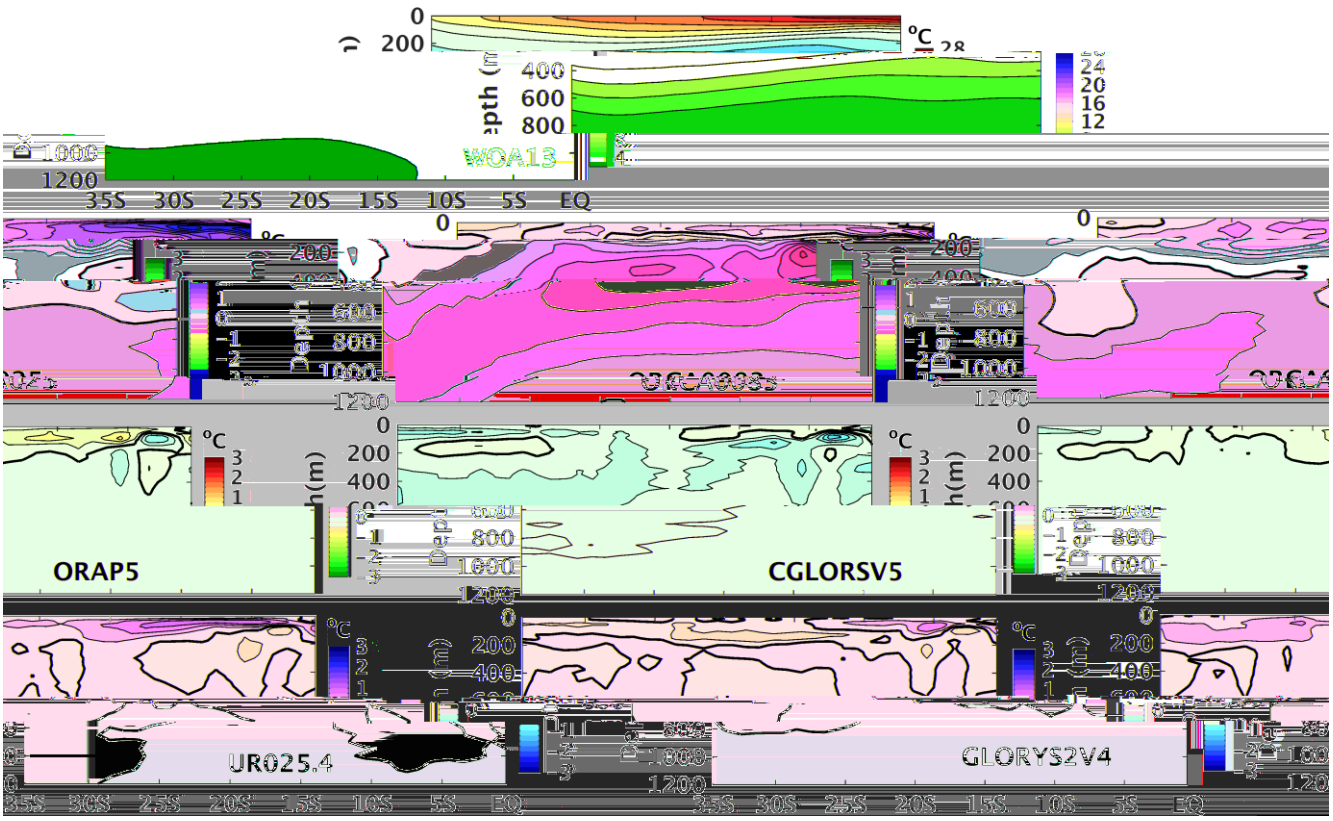

Figure 6. The zonal averaged temperature (˚C) as a function of latitude for WOA13 from 1995 to 2012 (top panel), followed by the zonal averaged temperature of each product from 1997-2010 minus WOA13. The ~~black~~ thick solid line represents the ~~contour of~~ 0˚C contour.

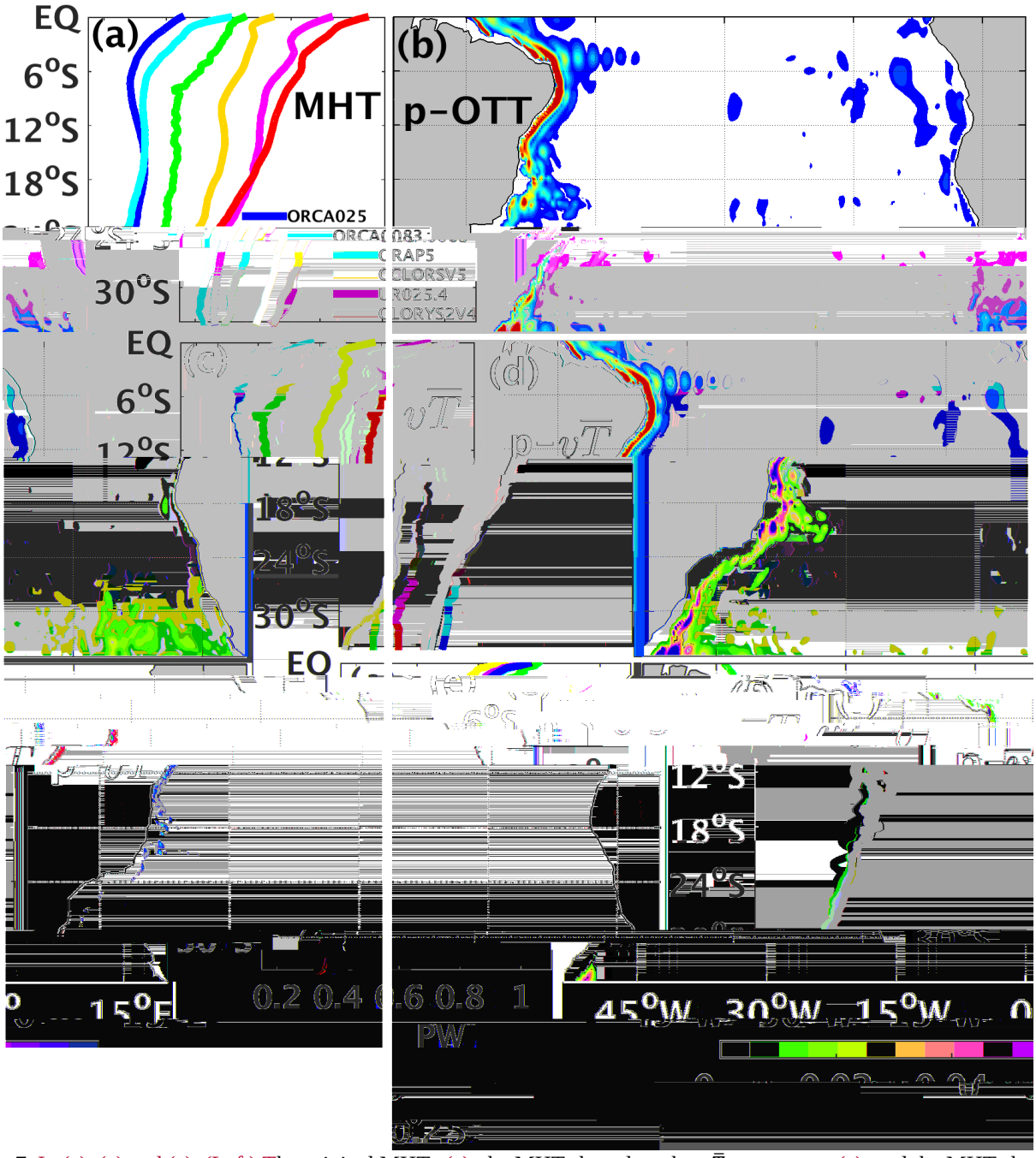

Figure 7. ~~In (a), (c) and (e),~~ (Left) The original MHTs (a), the MHTs based on the $v\bar{T}$ component (c), and the MHTs based on the $\bar{v}T$ component (e) in PW. ~~ are respectively shown. In (b), (d) and (f),~~ (Right) The ENS-ALL spread of the p-OTTs (b), p-$v\bar{T}$ (d) and p-$\bar{v}T$ (f) ~~are respectively presented with units of~~ in PWT per 0.25˚. Overbar represents the mean of the ~~ensemble of products means~~ENS-ALL.

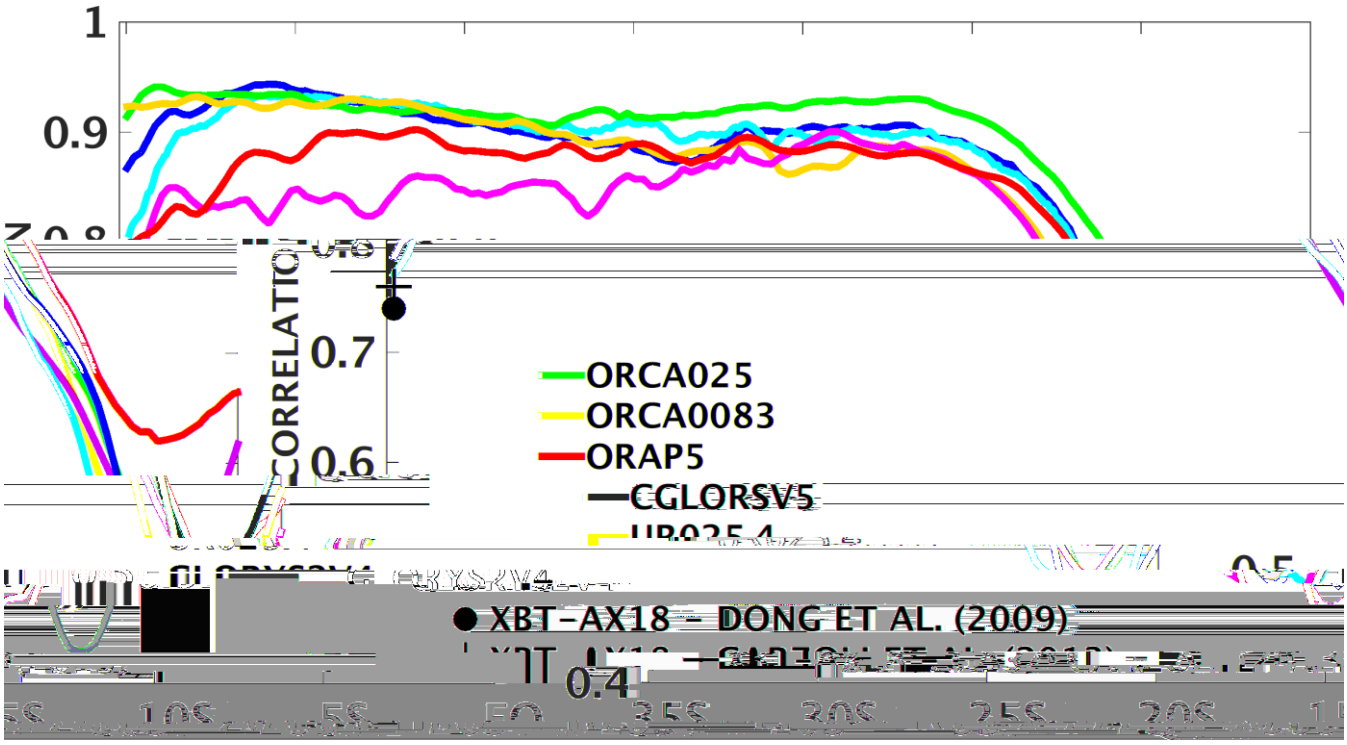

Figure 8. The monthly Pearson correlation between the SAMOC strength and the MHT as a function of latitude for 1997-2010, calculated with significance level of 95%. The quarterly XBT-AX18 correlation between the SAMOC strength and MHT at 35˚S is also included for comparisons. ~~The black solid line represents the correlation of 0.7.~~

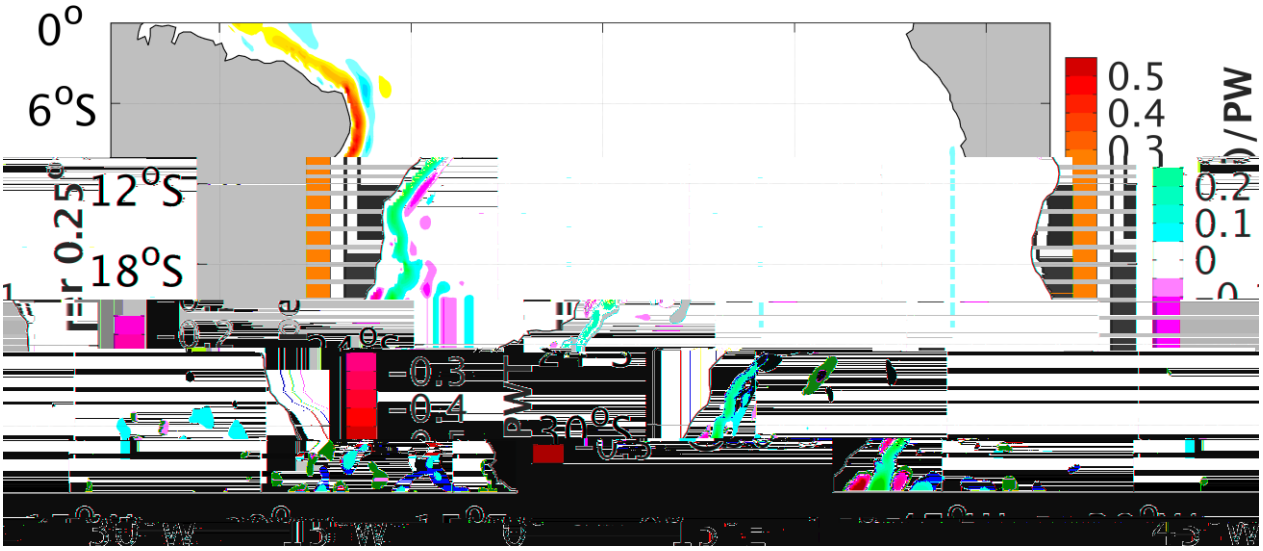

Figure 9. The linear regression coefficient between the inter-product p-OTTs and their MHTs for each latitude. Units are in PWT per 0.25˚ ~~out of~~per 1 PW~~,~~ across each latitude.

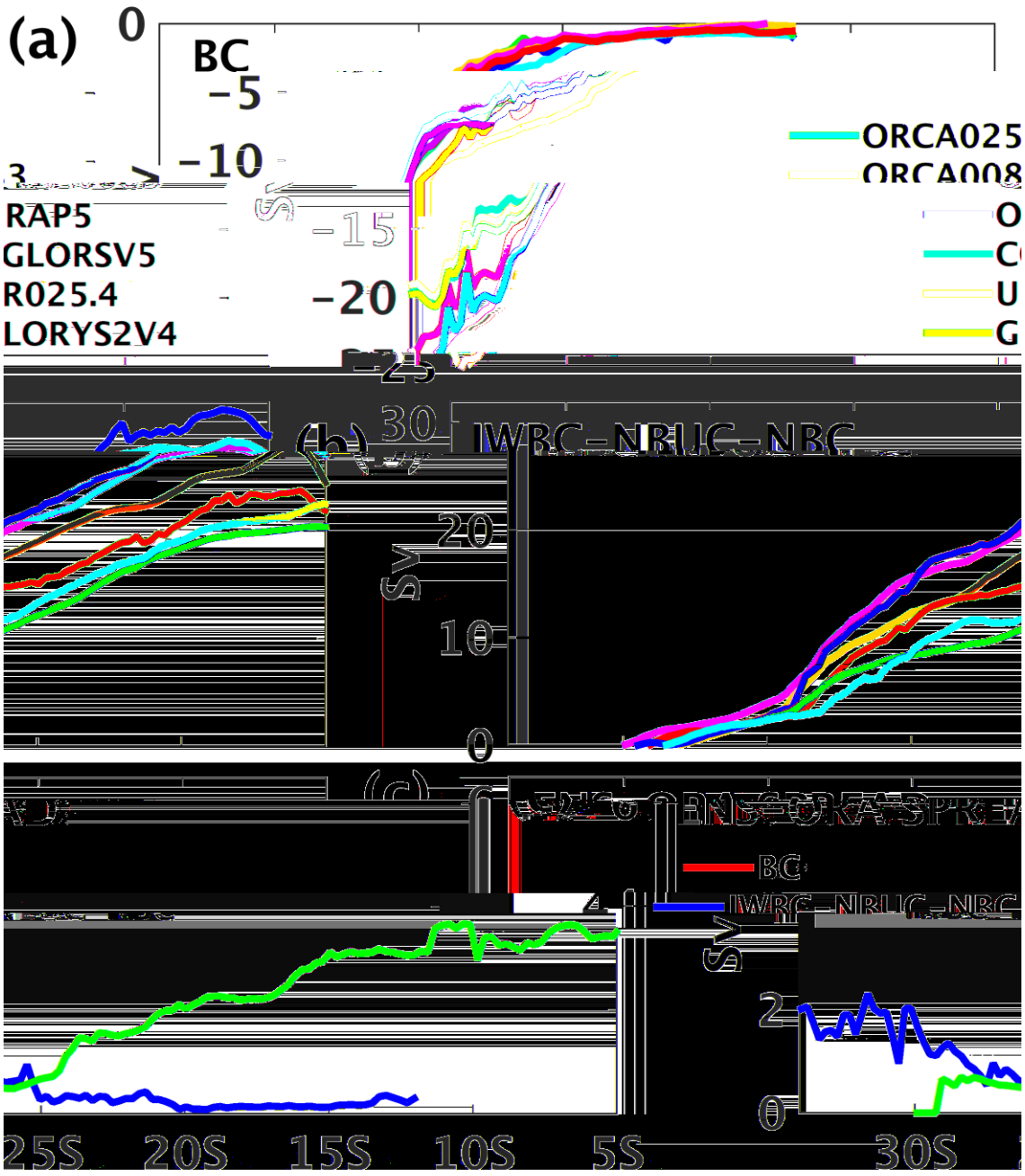

Figure 10. The transports (Sv) within 6˚ of the west coast for the (a) BC and (b) IWBC-NBUC-NBC system, following the isopycnal limits of the South Atlantic western boundary water masses as in Mémery et al. (2000) and Donners et al. (2005). The TW, SACW and AAIW limits are defined in kg m^{-3} with $\sigma < 25.5$, $25.5 \leq \sigma < 27.1$, and $27.1 \leq \sigma < 27.3$, respectively. The~~ir~~ ENS-ORA spread~~s~~ (Sv) of the western boundary current transports ~~(Sv)~~ are displayed in (c).

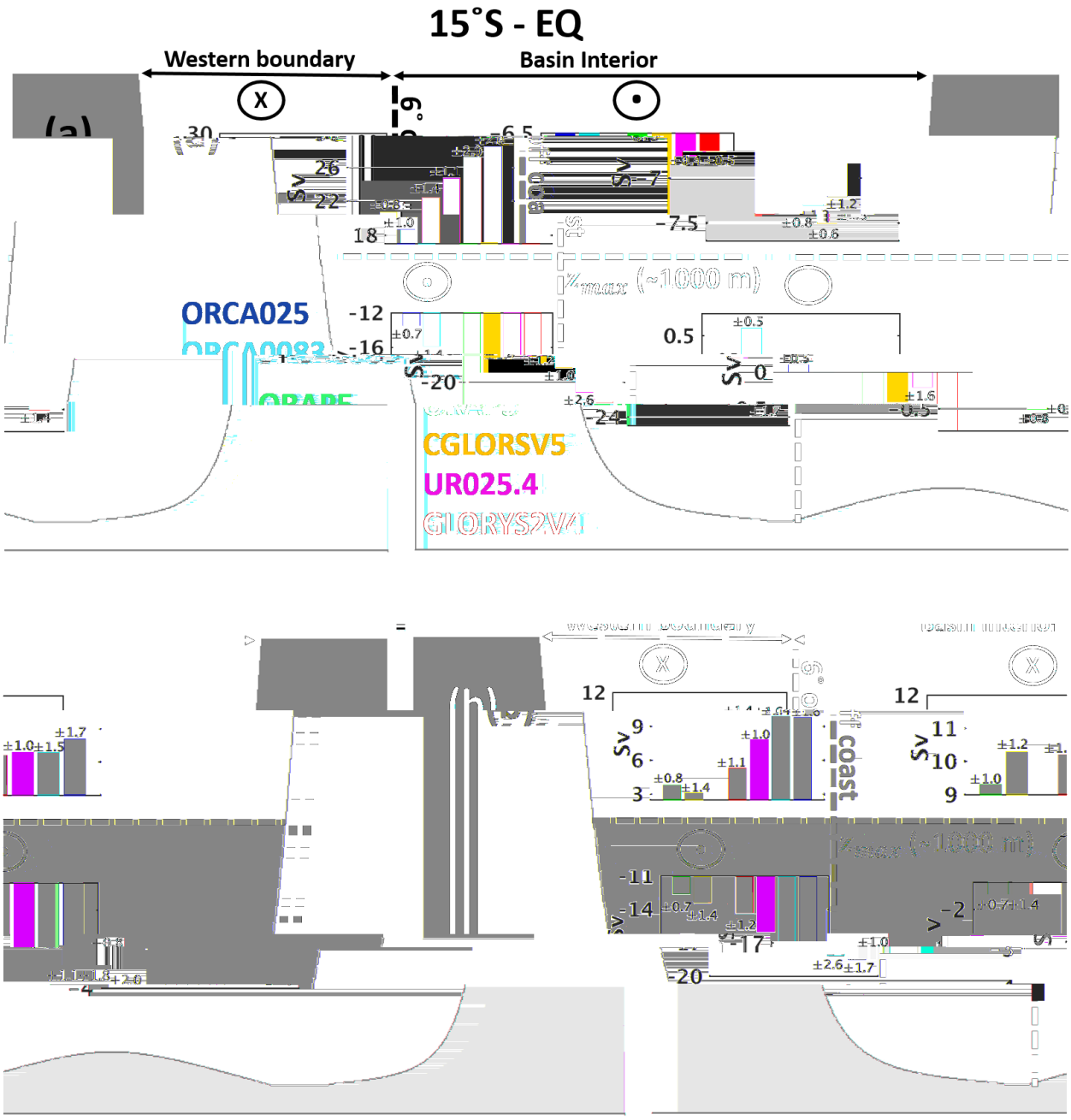

Figure 11. 4-box model of the averaged transports (1997-2010, in Sv) from (a) 15˚S to the equator, and from (b) 30˚S to 15˚S. 6˚ off the coast is chosen to separate the western boundary ~~and~~ from the basin interior.~~, as well as~~ The depth of maximum SAMOC z_{max} for each product is used to separate the upper and deep circulations. The circles with "x" and dots represent flow going into and out of the ~~screen~~page, respectively. The empty circle means that there is no agreement about the direction of the flow. ± corresponds to the interannual variability of each product~~, and units are in Sv.~~

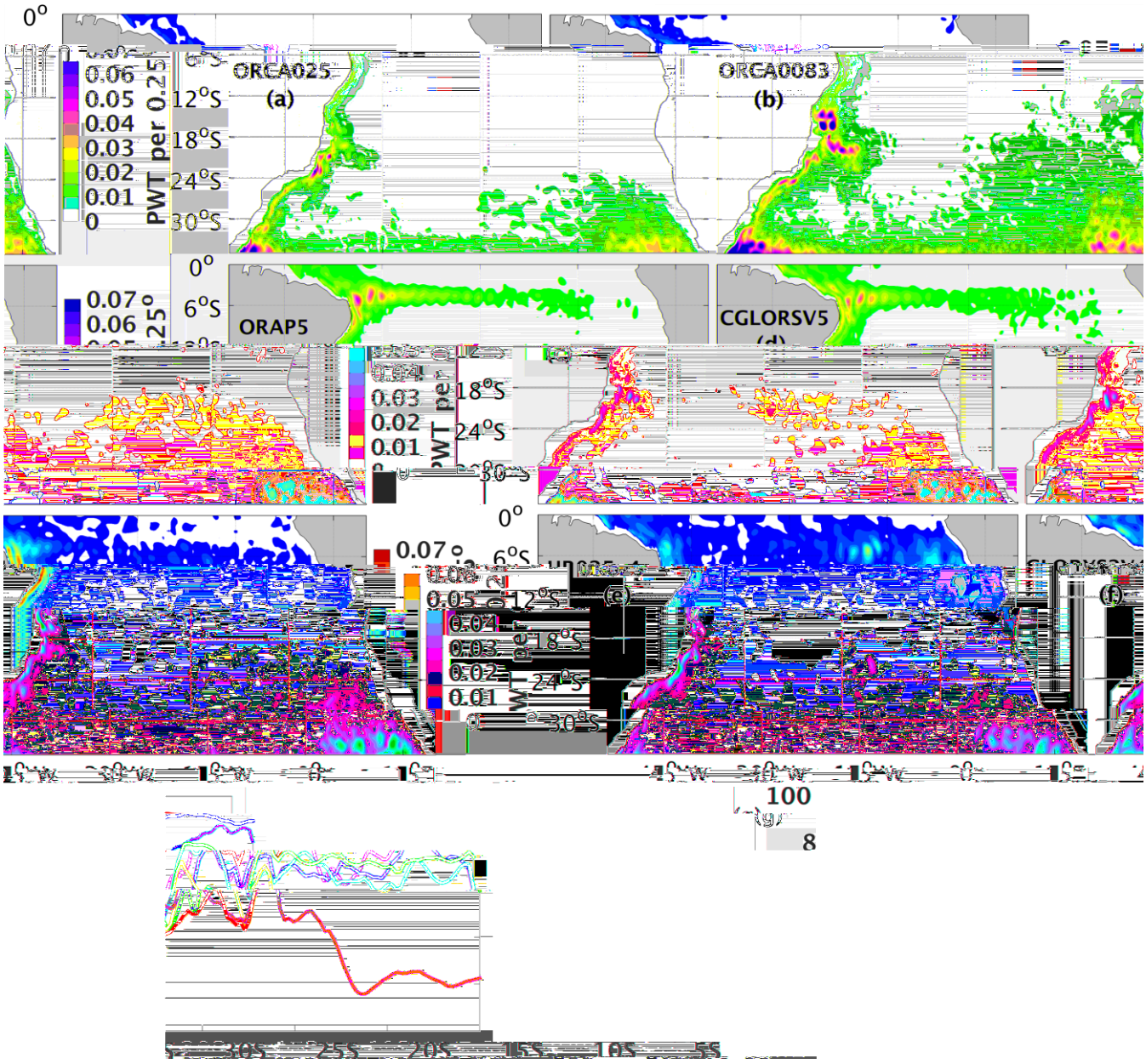

Figure 12. (a-f) Interannual p-OTT spread for the period 1997-2010. Units are in PWT per 0.25˚. In (g) the interannual p-OTTs variances for each product are summed within 6˚ of the west coast across each latitude and displayed as a percentage of the total MHT variance.

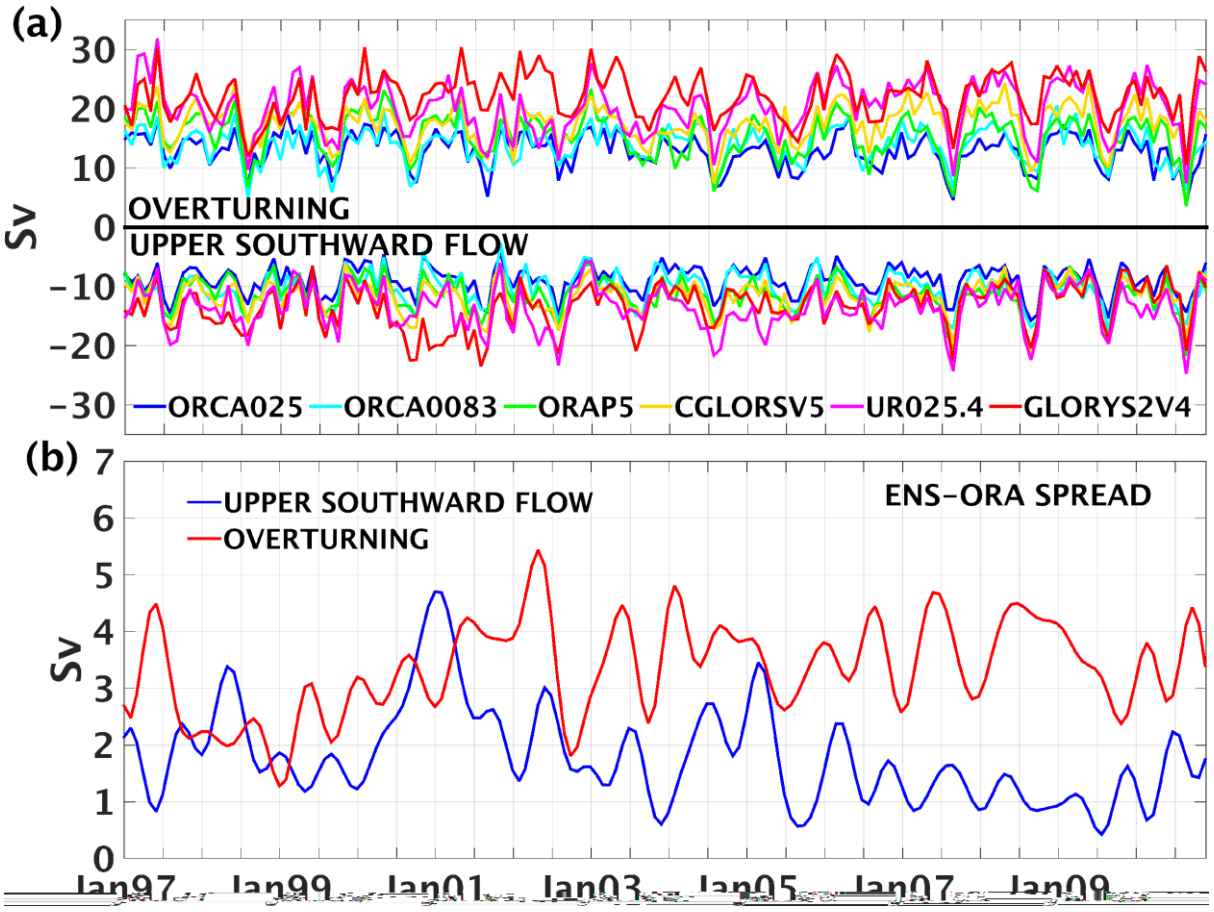

715

Figure 13. (a) Monthly time series of ψ_{max} (Sv) and the maximum upper southward flow (Sv) for each product calculated as an average from 15˚S to the equator, and. ~~In~~ (b) their~~their~~ ENS-ORA spreads (Sv) ~~are presented~~. A running mean of 6 months was applied to smooth the ENS-ORA spread time series. The upper southward flow is calculated using the same approach as in Fig. 4g.